Polyakov loop in 2+1 flavor QCD from low to high temperatures

A. Bazavov, N. Brambilla, H.-T. Ding, P. Petreczky, H.-P. Schadler, A. Vairo, and J. H. Weber

(TUMQCD Collaboration)

Phys. Rev. D **93**, 114502 — Published 3 June 2016

DOI: 10.1103/PhysRevD.93.114502

Polyakov loop in 2+1 flavor QCD from low to high temperatures

A. Bazavov[a], N. Brambilla[b,c], H.-T. Ding[d], P. Petreczky[e], H.-P. Schadler[e,f], A. Vairo[b], J. H. Weber[b,g]
(TUMQCD Collaboration)

[a] *Department of Physics and Astronomy, University of Iowa, Iowa City, Iowa 52242-1479, USA*
[b] *Physik Department, Technische Universität München, D-85748 Garching, Germany*
[c] *Institute of Advanced Studies, Technische Universität München, D-85748 Garching, Germany*
[d] *Key Laboratory of Quark & Lepton Physics (MOE) and Institute of Particle Physics, Central China Normal University, Wuhan 430079, China*
[e] *Physics Department, Brookhaven National Laboratory, Upton, NY 11973, USA*
[f] *Institute of Physics, University of Graz, 8010 Graz, Austria*
[g] *Exzellenzcluster Universe, Technische Universität München, D-85748 Garching, Germany*

We study the free energy of a static quark in QCD with 2+1 flavors in a wide temperature region, 116 MeV $< T <$ 5814 MeV, using the highly improved staggered quark (HISQ) action. We analyze the transition region in detail, obtain the entropy of a static quark, show that it peaks at temperatures close to the chiral crossover temperature and also revisit the temperature dependence of the Polyakov loop susceptibilities using gradient flow. We discuss the implications of our findings for the deconfinement and chiral crossover phenomena at physical values of the quark masses. Finally a comparison of the lattice results at high temperatures with the weak-coupling calculations is presented.

PACS numbers: 12.38.Gc, 12.38.-t, 12.38.Bx, 12.38.Mh

I. INTRODUCTION

As the temperature is increased, strongly interacting matter undergoes a transition to a state with different properties than the vacuum at zero temperature. Deconfinement of gluons and quarks, restoration of chiral symmetry and screening of color charges are the key properties of this thermal medium (for recent reviews see e.g. [1–3]).

The expectation value of the Polyakov loop is a sensitive probe of the screening properties of the medium. In SU(N) gauge theories the Polyakov loop is an order parameter for deconfinement. At the transition temperature, both the bare and the renormalized Polyakov loop exhibit a discontinuity and their fluctuations diverge. Hence, the bare Polyakov loop is used to study the deconfinement phase transition in SU(N) gauge theories, in particular the bare Polyakov loop susceptibility is used to define the phase transition temperature (see e.g. Ref. [4]). To what extent it is a sensitive probe of deconfinement in QCD with light dynamical quarks is not quite clear in view of the crossover nature of the transition [5]. In particular, it is not clear if it is possible to define a crossover temperature from the bare Polyakov loop, since it is a continuous quantity in the crossover region. In recent years the deconfinement transition in QCD with light dynamical quarks has been studied in terms of fluctuations and correlations of conserved charges, which indicate the appearance of quark degrees of freedom just above the chiral transition temperature [6–9].

After proper renormalization the expectation value of the renormalized Polyakov loop is related to the free energy, F_Q, of a static quark [10, 11]

$$L^{\rm ren} = \exp(-F_Q^{\rm ren}/T). \qquad (1)$$

The renormalized Polyakov loop, or equivalently the free energy of a static charge F_Q has been studied in SU(N) gauge theories in a wide temperature interval [11–15]. Comparisons of the lattice results with weak-coupling calculations have also been performed up to next-to-leading order (NLO) [16] and up to next-to-next-to-leading order (NNLO) [17].

The renormalized Polyakov loop has been computed in QCD with dynamical quarks for various quark flavor content and quark masses [18–26]. Continuum extrapolated results with physical quark masses exist for staggered fermion formulations [23, 25, 26]. For large quark masses continuum results are also available for overlap and Wilson fermion formulations [27, 28]. Unfortunately, none of the above studies extend to sufficiently high temperature to make contact with weak-coupling calculations.

The relation of the Polyakov loop to the nature of the QCD crossover remains unclear. For large quark masses the deconfinement crossover defined in terms of the Polyakov loop and the chiral crossover defined in terms of the chiral condensate happen at about the same temperature [18, 19, 29]. In the crossover region, both the Polyakov loop and the chiral condensate change rapidly and their fluctuations become large. For physical values of the quark masses the situation may be different. In Refs. [30, 31] it was found that the deconfinement crossover defined in terms of the renormalized Polyakov loop happens at temperatures significantly higher than the chiral crossover temperature defined as the maximum of the chiral susceptibility. The study of ratios of fluctuations of the imaginary and real parts of the Polyakov loop in Ref. [32] suggested that the deconfinement and chiral crossover happen at about the same temperature. However, as this study used an ad-hoc renormalization prescription, lacked continuum extrapolation and provided

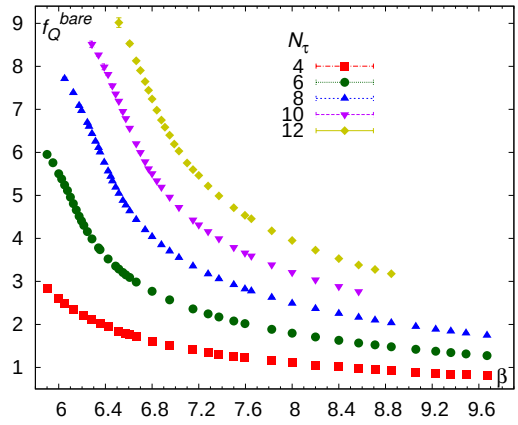

FIG. 1. (Color online) The bare free energy of a static quark $f_Q^{\rm bare} = F_Q^{\rm bare}/T = -\log L^{\rm bare}$ as function of the gauge coupling β for different N_τ values.

no information on the cutoff effects in full QCD, the implications of this result are not conclusive.

In this paper we will study the free energy of a static quark in a broad temperature region extending to 5.8 GeV. We will also re-examine the behavior of F_Q in the transition region, in particular, we will calculate the entropy of a static quark, $S_Q = -\partial F_Q/\partial T$, and discuss its relation to the deconfinement transition temperature. We will show that the deconfinement transition temperature, defined at the peak of S_Q, is actually consistent with the chiral transition temperature.

The rest of the paper is organized as follows. In Section II we discuss our lattice setup. In Section III we discuss the renormalization of the Polyakov loop using the static quark anti-quark energy at zero temperature. In Section IV our results on the entropy of a static quark will be presented. Section V will show how to extend the lattice calculations of the static quark free energy to higher temperatures. In Section VI we will discuss the calculation of the renormalized Polyakov loop and its susceptibility using the gradient flow. The free energy of a static quark in the high temperature region will be compared to the weak-coupling results in Section VII. Finally, Section VIII contains our conclusions. Some technical details of the calculations will be given in the appendices.

II. LATTICE QCD SETUP

We perform calculations of the bare Polyakov loop at non-zero temperature on $N_\sigma^3 \times N_\tau$ lattices with $N_\tau = 4,\ 6,\ 8,\ 10$ and 12, and the aspect ratio of $N_\sigma/N_\tau = 4$ using the highly improved staggered quark (HISQ) action [33]. The gauge configurations have been generated by the HotQCD Collaboration [24, 34], in the course of studies of quark number susceptibilities at high temperatures [35, 36] as well as in a previous study of the renormalized Polyakov loop with the HISQ action [25].

We required additional gauge configurations and generated these using the SuperMUC and C2PAP computers at Leibniz Rechenzentrum (LRZ) in Garching. Additional gauge configurations have been generated for $N_\tau = 4,\ 6$ and 8 to calculate the Polyakov loop at very high temperatures. Further gauge configurations have been generated for $N_\tau = 10$ and 12 to reduce uncertainties of the free energy at low temperatures and achieve sufficient resolution of the peak of S_Q.

The gauge configurations have been generated in the range of gauge coupling $\beta = 5.90 - 9.67$ with $\beta = 10/g_0^2$ using the rational hybrid Monte-Carlo (RHMC) algorithm and the MILC code. Details on the HISQ action implementation in the MILC code can be found in [37]. The lattice spacing a has been fixed by the r_1 scale and we use the parameterization of r_1/a given in Ref. [34]. Using this parameterization we find that the above β range corresponds to a temperature range of 116 MeV $< T <$ 5814 MeV. The Polyakov loop has been calculated after each molecular dynamic time unit (TU). For temperatures $T < 407$ MeV the accumulated statistics corresponds to $30 - 60$ thousands of TUs. At higher temperatures in many cases far fewer gauge configurations are available. The details on collected statistics are given in Appendix A.

The Polyakov loop on the lattice is defined as

$$P(\mathbf{x}) = \frac{1}{3}\mathrm{Tr}\prod_{x_0=0}^{N_\tau-1} U_0(\mathbf{x}, x_0), \qquad (2)$$

where $U_\mu(x = (\mathbf{x}, x_0))$ are the lattice link variables. The bare expectation value of the Polyakov loop will be denoted by $L^{\rm bare}$ in what follows, $L^{\rm bare} = \langle P \rangle$. Since the expectation value of the Polyakov loop is independent of $\mathbf{x}$ we average the Polyakov loop over the entire spatial volume. Our results for the bare Polyakov loop are summarized in Fig. 1 in terms of the scaled bare static quark free energy $f_Q^{\rm bare} = -\log L^{\rm bare}$ as a function of the gauge coupling β. Here and in what follows we denote by $f_Q^{\rm bare}$ the scaled bare free energy of a static quark, $f_Q^{\rm bare} = F_Q^{\rm bare}/T$. As one may see from the figure, $f_Q^{\rm bare}$ decreases for increasing β and for decreasing N_τ. The continuum limit at fixed temperature would be reached by varying N_τ and β simultaneously in the limit $N_\tau \to \infty$, following lines going from the lower left corner into the direction of the upper right corner. Since $f_Q^{\rm bare}$ diverges as one proceeds along these lines, the continuum limit of $f_Q^{\rm bare}$ is not defined. Thus, we must subtract this divergence before taking the continuum limit. We will discuss this in the next section.

III. RENORMALIZATION OF THE POLYAKOV LOOP AND THE CONTINUUM EXTRAPOLATION

The Polyakov loop needs multiplicative renormalization [38]. This means that the free energy of a static

quark F_Q needs an additive renormalization. The additive renormalization of F_Q is related to the additive renormalization of the energy of a static quark anti-quark ($Q\bar{Q}$) pair at zero temperature. The static quark anti-quark free energy $F_{Q\bar{Q}}(r,T)$ agrees with the static quark anti-quark energy at zero temperature at short distances once a finite additive term due to trivial color factors is included [11]. On the other hand $F_{Q\bar{Q}}(r\to\infty,T) = 2F_Q(T)$ [10, 11]. Therefore, the renormalization constant of F_Q, which we denote by C_Q, is half of the renormalization constant of the static energy at zero temperature.

To determine the normalization constant C_Q we require that the static $Q\bar{Q}$ energy for zero temperature at a distance $r = r_0$ is equal to $0.954/r_0$ [24]. This normalization condition is equivalent to normalizing the static energy to $0.2065/r_1$ [34] at a distance $r = r_1$. Normalizing the static energy at r_1, i.e. at shorter distances has the advantage of reducing the statistical errors at large β, while the normalization at distance r_0 is more suitable for coarser lattices, i.e. smaller values of β. Using the lattice results on the static $Q\bar{Q}$ energy from Ref. [24] and normalizing them to $0.954/r_0$ for $\beta \leq 6.488$ we determine $r_0 C_Q$. Then using the results on the static $Q\bar{Q}$ energy at higher β from Refs. [24, 34] and normalizing those to $0.2065/r_1$ we determine $r_1 C_Q$. Finally using r_1/a and r_0/a from Refs. [24, 34] we calculate the values of the normalization constant in lattice units $aC_Q(\beta) = c_Q(\beta)$ which are shown in Fig. 2 and tabulated in Appendix A. Note that since C_Q has a $1/a$ divergence, c_Q is finite and is a slowly varying function of β. Once the cutoff dependence is rephrased in terms of the lattice spacing $a(\beta)$, we may write $C_Q = b/a + c + \mathcal{O}(a^2)$. The divergence b/a cancels against the divergence of the bare free energy. The constant c is a scheme dependent constant, which depends on the distances r_0 or r_1, but is independent of the lattice spacing. Since the leading higher order corrections are suppressed by $\alpha_s a^2$ for the HISQ/Tree action, the derivative in a of these corrections vanishes in the continuum limit. We note that, since $T = 1/(aN_\tau)$, at fixed N_τ the dependence of c_Q on a translates into a dependence on the temperature.

Now for the renormalized free energy in temperature units we can write

$$f_Q^{\rm ren}(T(\beta,N_\tau),N_\tau) = f_Q^{\rm bare}(\beta,N_\tau) + N_\tau c_Q(\beta). \qquad (3)$$

The renormalized free energy depends on β through the chain rule for $T(\beta,N_\tau)$. We use T as argument instead of β, since the continuum limit of $f_Q^{\rm ren}(T(\beta,N_\tau),N_\tau)$ can be taken for fixed temperature. Hereafter, we usually omit the superscript "ren" when referring to renormalized quantities, but keep the superscript "bare" for the bare quantities. Here and in what follows we denote by f_Q the scaled renormalized free energy of a static quark, $f_Q = F_Q/T$. In order to determine $f_Q^{\rm bare}$ and c_Q as a function of β and/or as a function of the temperature, we interpolate the lattice results on $c_Q(\beta)$ and $f_Q^{\rm bare}(\beta,N_\tau)$ independently in β.

First, we discuss the interpolation procedure for c_Q. To

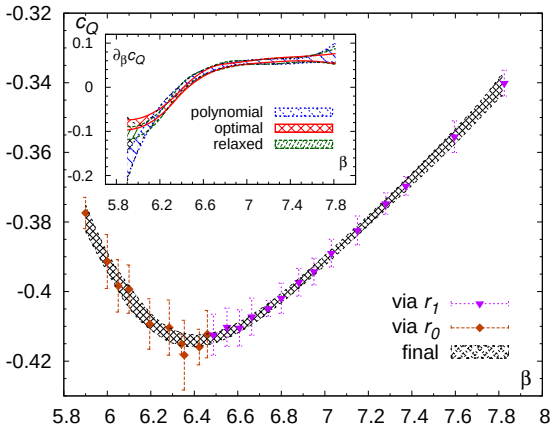

FIG. 2. (Color online) Renormalization constant $c_Q(\beta)$ from the $Q\bar{Q}$ renormalization procedure. Interpolations are shown as 1σ bands and data points are explained in the text. The inset shows the derivative $\frac{\partial c_Q}{\partial \beta}$. Optimal and relaxed refer to different spline interpolations with $n_k = 4$ or $n_k = 5$ knots respectively.

obtain c_Q as a function of β we use smooth splines and polynomial interpolations. The errors on the interpolations have been estimated using the bootstrap method. We varied the number of knots of the splines as well as the value of the smoothing parameter in order to estimate the systematic errors. In the case of polynomial fits we consider polynomials of different degree. The interpolation of c_Q is also shown in Fig. 2. In the inset of the figure we show the derivative of c_Q with respect to beta in order to highlight the spread in different interpolations. The differences between the different interpolations are most visible in the β dependence of the derivative of c_Q that is needed for the e valuation of the entropy of a static charge to be discussed in the next section.

Next, we discuss the interpolations of the free energy as well as the continuum extrapolations. At finite cutoff, the temperature T is related to N_τ and the lattice spacing a through $aN_\tau = 1/T$; trading a for β we can also write $\beta = \beta(T,N_\tau)$. Consequently, the limit $a \to 0$ at fixed temperature is tantamount to the limit $N_\tau \to \infty$. The power law dependence of cutoff effects on a or $1/N_\tau$ respectively is determined by the leading discretization errors of the lattice simulations ($\mathcal{O}(\alpha_s a^2, a^4)$ for the HISQ action). We will use two approaches to do this, which we will call local and global extrapolations. In the first approach, which we will call a local fit, we perform the interpolation of the lattice results for $f_Q^{\rm bare}$ as function of β for each N_τ separately. Using the value of c_Q determined above we then calculate the renormalized free energy $f_Q(T(\beta,N_\tau),N_\tau)$ for each N_τ and perform continuum extrapolations. In the second approach, which we will call a global fit, we simultaneously fit the temperature and N_τ dependence of $f_Q^{\rm bare}(\beta,N_\tau) + N_\tau c(\beta)$. Setting $N_\tau \to \infty$ in the resulting fit we obtain the continuum extrapolated results for the renormalized free energy. We will discuss these two approaches in the following subsec-

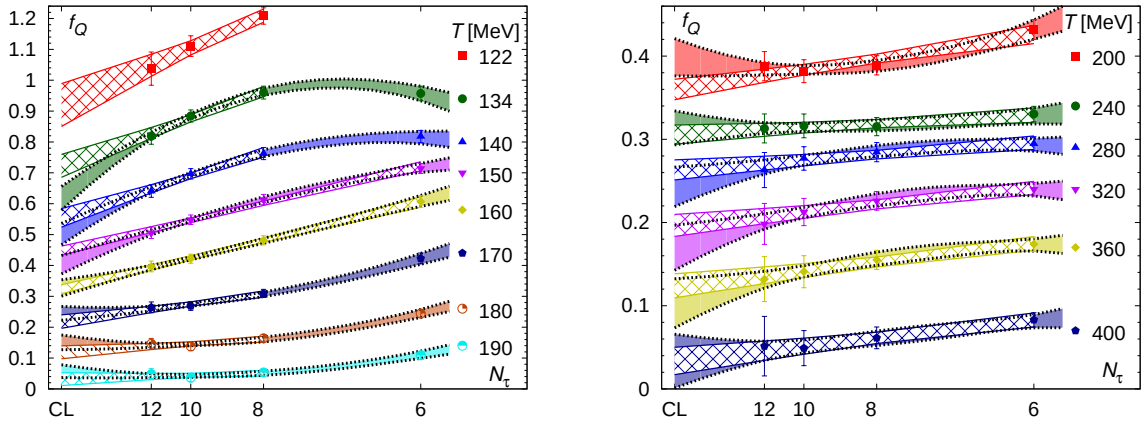

FIG. 3. (Color online) The static quark free energy at various temperatures as function of N_τ. 'CL' marks the continuum limit ($N_\tau \to \infty$). Results for each temperature are shifted by some constant for better visibility. The $1/N_\tau^2$ continuum extrapolations are shown as bands with filled pattern. The continuum extrapolations with $1/N_\tau^4$ term included are shown as solid filled bands. The width of the band shows the statistical uncertainty of the fits. The left panel shows the results in the low temperature region, while the right panel shows the results in the high temperature region.

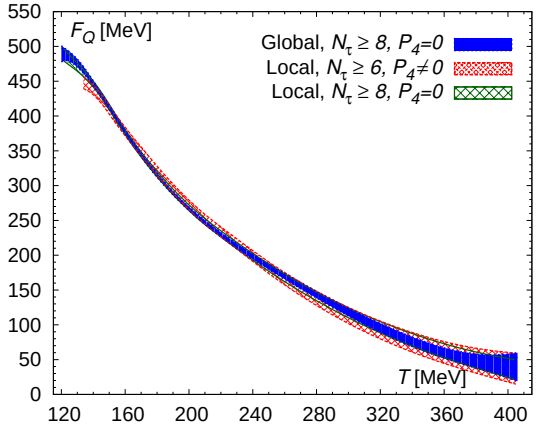

FIG. 4. (Color online) Different continuum extrapolations for the static quark free energy F_Q. We show extrapolations with coefficient P_4/N_τ^4 term set to zero as well as for non-zero values of the coefficient P_4.

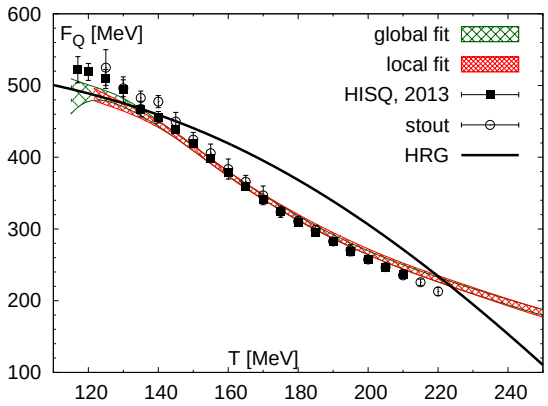

FIG. 5. (Color online) The continuum results for the free energy of static quark compared to previous calculations [23, 25]. Also shown as a solid black line is the hadron resonance gas calculation of F_Q from Ref. [25].

tions in more details.

A. Local interpolations and extrapolations

To perform the interpolation of $f_Q^{\rm bare}(\beta, N_\tau)$ we split the β range in overlapping low β and high β intervals which roughly correspond to temperatures $T < 200$ MeV and $T > 200$ MeV respectively. In these intervals for each N_τ we perform interpolations in β using smoothing splines as well as polynomial fits. We find that in the low beta range it is sufficient to use splines with $5-7$ knots, while in the high β range we use splines with $8-19$ knots depending on the value of N_τ. The statistical errors of the interpolations are estimated using the bootstrap method. To estimate possible systematic errors in the interpolation we also performed polynomial fits of the lattice data for $f_Q^{\rm bare}(\beta, N_\tau)$ in the above intervals. We find that the interpolations obtained with polynomials and splines agree well within the estimated statistical errors not only for $f_Q^{\rm bare}(\beta, N_\tau)$ but also for its derivative. Therefore, there are no additional systematic errors in our analysis. The details of the interpolations and fits are presented in Appendix B. Having the interpolation for $f_Q^{\rm bare}(\beta, N_\tau)$ and the interpolation for c_Q we calculate the renormalized free energy for each N_τ. We then perform a $1/N_\tau^2$ extrapolation for f_Q to obtain the continuum limit for each value of the temperature. In Fig. 3 we show the N_τ dependence of f_Q together with $1/N_\tau^2$ and $1/N_\tau^4$ extrapolations. As one can see from the figure cutoff effects are fairly small for $T > 200$ MeV and $1/N_\tau^2$ holds including $N_\tau = 6$ data. Note that we do

not consider the $N_\tau = 4$ results partly because they are available only for $T > 200$ MeV and partly because they are outside the scaling window. At lower temperature cutoff effects are larger and the $N_\tau = 6$ data are not in the scaling regime. Therefore, we have to consider fits with $1/N_\tau^4$ term included, or use $1/N_\tau^2$ fits for $N_\tau \geq 8$ only. The continuum results obtained with the above extrapolations are shown in Fig. 4.

B. Global fits and extrapolations

In the previous subsection we have seen that the temperature dependence can be described by polynomials in the low and high beta ranges once β has been reexpressed in T. Furthermore, the N_τ dependence of the lattice results is well described by a function $P_0+P_2/N_\tau^2+P_4/N_\tau^4$. Therefore, we performed fits for $N_\tau = 6,\ 8,\ 10$ and 12 data on $f_Q(T(\beta, N_\tau), N_\tau)$ using the following form

$$P_0(T) + \frac{P_2(T)}{N_\tau^2} + \frac{P_4(T)}{N_\tau^4}. \tag{4}$$

Here $P_i,\ i = 0, 2, 4$ are polynomials in the temperature T. As we did for local interpolations, we split the temperature range in overlapping low and high temperature intervals and performed the global fits in both intervals separately. These intervals roughly correspond to $T < 200$ MeV and $T > 200$ MeV. The low temperature fits extend only down to the lowest temperatures where bare free energies are available for $N_\tau = 12$, which is slightly above 120 MeV. The high temperature fits extend only up to the highest temperature where c_Q is available for $N_\tau = 12$, which is slightly below 410 MeV. We used fits with and without the $1/N_\tau^4$ term, as well as including and excluding the $N_\tau = 6$ data. We find that within estimated statistical errors all the fits agree both for $f_Q(T(\beta, N_\tau), N_\tau)$ and its derivatives. The account of these fits is given in appendix B. For the continuum result we use the fit which does not include the $N_\tau = 6$ data and has fixed $P_4 = 0$. We consider this fit as our continuum limit after setting $N_\tau = \infty$, which corresponds to setting $P_2 = 0$ in the resultant fit function. This is shown in Fig. 4, where we see that local and global continuum extrapolations for f_Q agree very well.

C. Comparison with previous calculations

Now let us compare the above continuum results with the previously published results that use the same renormalization scheme with improved staggered quark actions. Namely we compare our results with the continuum results obtained with the stout action [23] as well as with the HISQ action [25]. This comparison is shown in Fig. 5. We see that our results agree with the previously published results within errors, however, the central values for F_Q in our analysis are slightly smaller for $T < 130$ MeV due to different way the continuum extrapolation is performed. The previous estimate of the continuum limit for $T \leq 135$ MeV had been performed by averaging $N_\tau = 10$ and $N_\tau = 8$ data [25], whereas our analysis includes new $N_\tau = 12$ ensembles at low temperatures that made a controlled continuum extrapolation possible. For $T > 180$ MeV the central value of F_Q in our analysis is somewhat larger. This is due to the updated value of the renormalization coefficients c_Q. The previous HISQ calculations relied on the zero temperature static quark anti-quark energies obtained in Ref. [24], which have larger statistical uncertainty and use fewer β values. The current analysis of c_Q is based on the analysis of the zero temperature static quark anti-quark energies from Ref. [34], which has higher statistics and uses more β values. The main new element in our analysis is that it extends to significantly higher temperatures.

Finally, we compare our results with the prediction of the hadron resonance gas (HRG) calculation for F_Q [25], which includes the contribution of all static-light mesons and all the static-light baryons (see also Ref. [39]). Since the HRG value of F_Q is only defined up to a temperature independent constant, this constant needs to be fixed. We do so by matching the HRG value of F_Q to the lattice results at lowest temperature. The comparison is shown in Fig. 5. We see that the HRG description works only for temperature $T < 140$ MeV which is in agreement with the previous analysis [25].

IV. ENTROPY OF A STATIC QUARK

While the free energy of a static quark encodes the screening properties of the hot QCD medium its temperature dependence is relatively featureless. The change in the screening properties of the medium can be seen more clearly in terms of the entropy of a static quark

$$S_Q(T) = -\frac{\partial F_Q(T)}{\partial T}. \tag{5}$$

Note that the equality holds also if the temperature derivative is taken at changing volume, since the pressure exerted by a static quark is zero. The entropy was discussed recently in connection with the strongly coupled nature of quark gluon plasma [41, 42]. The entropy of a static quark in SU(3) gauge theory diverges at the phase transition temperature and was considered in Ref. [40, 43]. The entropy was also calculated for 2 and 3 flavor QCD with larger than physical quark masses [18, 40]. It has a peak at the crossover temperature, i.e. it corresponds to the inflection point of F_Q. Therefore, calculating S_Q for the physical quark masses is of interest, since S_Q could be used to define a deconfinement transition temperature.

Based on the interpolation of f_Q and c_Q described in the previous section it is straightforward to estimate S_Q.

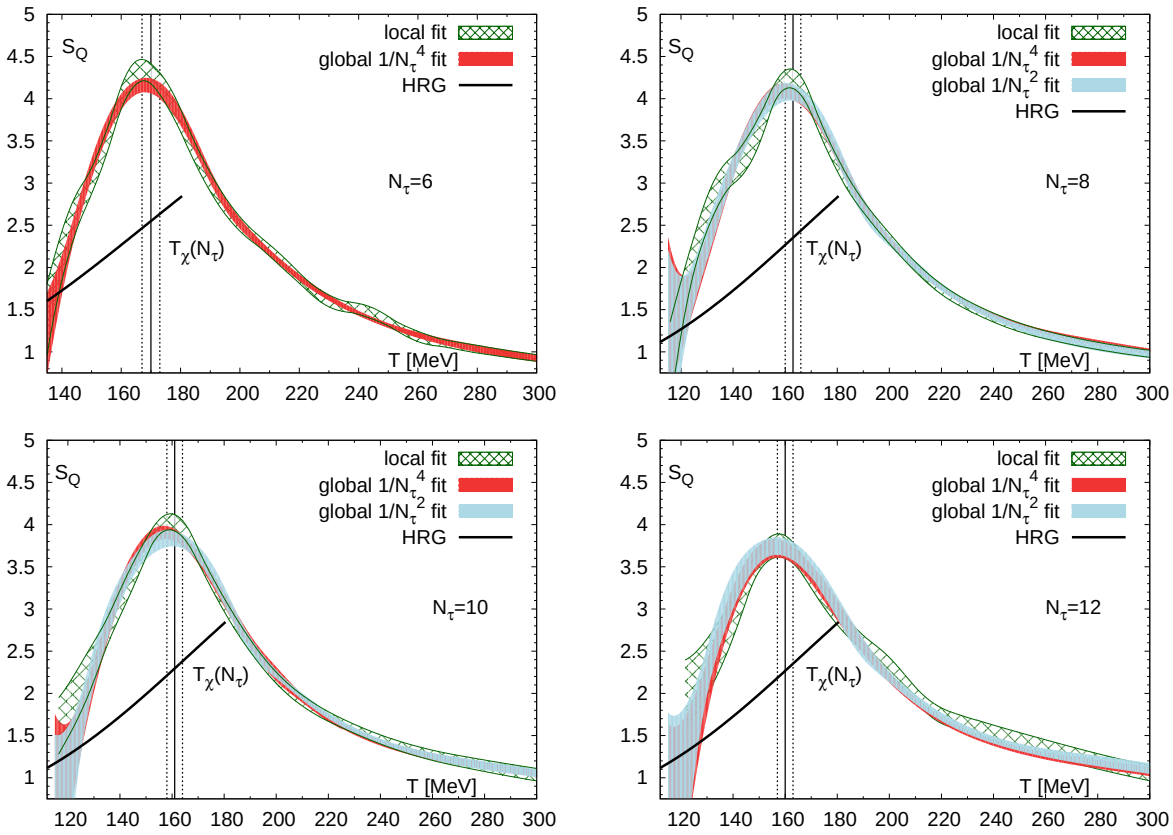

FIG. 6. (Color online) The entropy of a static quark calculated on $N_\tau = 6$, 8, 10 and 12 lattices. Shown are the results obtained from local and global fits. The vertical band corresponds to the chiral transition temperature from [24]. The solid black lines show the entropy in the hadron resonance gas model [25].

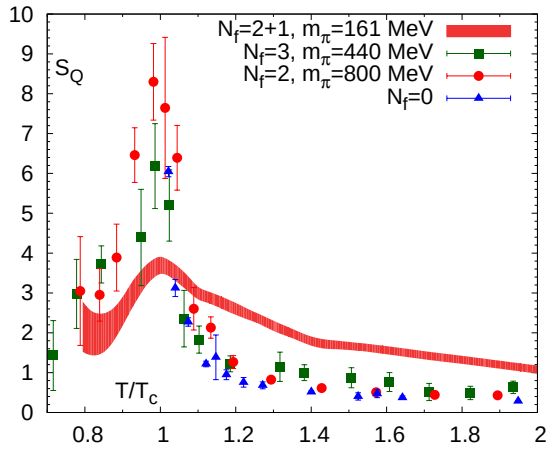

FIG. 7. (Color online) The comparison of S_Q in the continuum limit with previous calculations obtained on $N_\tau = 4$ lattices[18, 40]. The temperature axis has been rescaled for each lattice calculation by a corresponding lattice result for T_c, namely $T_S = 153\,\mathrm{MeV}$ for our result, $T_\chi = 193\,\mathrm{MeV}$ and $T_\chi = 200\,\mathrm{MeV}$ for the $N_f = 3$ and $N_f = 2$ results repectively and $T_L = 270\,\mathrm{MeV}$ for the quenched case ($N_f = 0$).

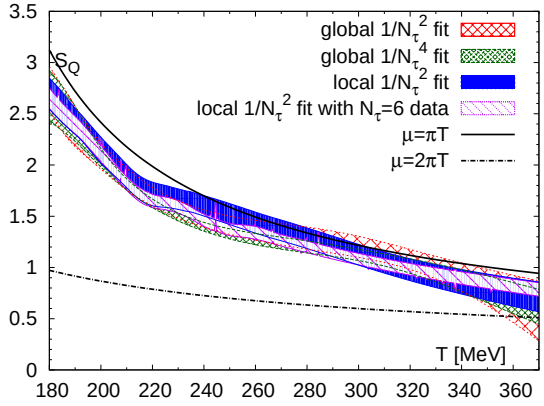

FIG. 8. (Color online) The entropy of a static quark in the high temperature region. The lines correspond to leading order weak-coupling calculations for scale $\mu = 2\pi T$ and $\mu = \pi T$.

We write

$$-S_Q = f_Q^{\mathrm{bare}} + T\frac{\partial\beta}{\partial T}\frac{\partial f_Q^{\mathrm{bare}}}{\partial\beta} + N_\tau(c_Q + T\frac{\partial\beta}{\partial T}\frac{\partial c_Q}{\partial\beta}). \quad (6)$$

Here, the derivative $\partial\beta/\partial T$ is related to the non-

perturbative beta function R_β through $R_\beta = T(\partial\beta/\partial T)$, determined in Ref. [34]. The entropy can also be calculated using the global fits for $f_Q(T(\beta, N_\tau), N_\tau)$ discussed in the previous section.

The numerical results for the entropy of a static quark are shown in Fig. 6 for $N_\tau = 6$, 8, 10 and 12 with local as well as global fits. These fits have been discussed in Sections III A and III B. We see that with increasing temperature S_Q increases reaching a maximum at some temperature and then decreases again. Therefore, it makes sense to discuss the behavior of the entropy at low temperatures, in the peak region and at high temperatures separately. Since S_Q for $N_\tau = 6$ is not in the a^2 scaling regime in the peak region and below, no a^2 scaling fit is shown for $N_\tau = 6$.

At low temperatures we expect S_Q to be described by the HRG model of Ref. [25], discussed in the previous section. The HRG predictions from this model for S_Q are shown as black lines in Fig. 6. For low temperatures $T < 130$ MeV our lattice results for S_Q overlap with the HRG curve. As the temperature increases we see very clear deviations from the HRG result, namely the entropy S_Q calculated on the lattice is significantly larger than the HRG prediction.

As mentioned above the entropy shows a peak at some temperature. The position of the maximum in S_Q turns out to be up to 3 MeV below the chiral crossover temperature at finite cutoff, $T_\chi(N_\tau)$ [24], which is shown as a vertical line in the figure for each N_τ separately. The bands indicate the uncertainty in $T_\chi(N_\tau)$. The values of $T_\chi(N_\tau)$ are obtained from the $O(2)$ scaling fits of the chiral susceptibilities [24]. If the maximum in the entropy of a static quark is used to define a deconfinement crossover temperature one could say that deconfinement and chiral crossover happen at about the same temperature.

We extrapolate to the continuum with different local and global fits, either including a P_4/N_τ^4 term (cf. Sec. III B) and $N_\tau = 6$ data or excluding both. The position of the peak scatters in the range 150.5 MeV $\leq T \leq$ 157 MeV, depending on the details of the fits, which are discussed in appendix B. We consider the local fit excluding P_4 and $N_\tau = 6$ as our final result and find the maximum of S_Q at $T_S = 153^{+6.5}_{-5}$ MeV. We estimate a systematic uncertainty of T_S as $^{+4}_{-2.5}$ MeV from the spread of the fits, which is smaller than the statistical errors that we quote.

The deconfinement transition temperature was defined as the inflection point of the renormalized Polyakov loop in Refs. [5, 31] and values of $T_L = 171(3)(4)$ MeV[1] and $T_L = 170(4)(3)$ MeV have been found, respectively. These values are significantly larger than the chiral transition temperature. The most likely reason for this is that the inflection point of the renormalized Polyakov loop depends on the renormalization condition and could be different from the inflection point of F_Q. The inflection point of the renormalized Polyakov loop can be obtained from the equation

$$\begin{aligned} 0 =& \frac{1}{L^{\rm ren}} \frac{\partial^2 L^{\rm ren}}{\partial T^2} = \left(\frac{\partial f_Q}{\partial T}\right)^2 - \left(\frac{\partial^2 f_Q}{\partial T^2}\right) \\ =& \frac{1}{T}\left(\frac{(f_Q + S_Q)^2 - 2(f_Q + S_Q)}{T} + \left(\frac{\partial S_Q}{\partial T}\right)\right), \end{aligned} \quad (7)$$

whereas the inflection point of the free energy F_Q is obtained from $0 = \partial S_Q/\partial T$. In other words, the two inflection points of the Polyakov loop and the free energy would agree if and only if $f_Q + S_Q = 0$ or 2. This would be the case if weak-coupling relation, $S_Q \simeq -f_Q$, was correct close to the crossover point. Instead, in support of the findings in Refs. [5, 31] we find the inflection point of the renormalized Polyakov loop significantly above the chiral transition temperature, between 180 and 200 MeV for each $N_\tau = 12$, 10, 8 and 6. Systematic uncertainties for $N_\tau = 12$ are underestimated by the error in this range (cf. appendix B). Eq. (7) shows that the inflection point of $L^{\rm ren} = \exp(-f_Q)$ depends on the term c of c_Q (cf. Sec. III) through f_Q and f_Q^2. For F_Q the change in the renormalization condition does not affect its inflection point in the continuum limit, which, in fact, does not depend on c.

We also compare our continuum results for S_Q with previous calculations obtained at much larger quark masses and $N_\tau = 4$ lattices [18, 40]. This comparison is shown in Fig. 7. The temperature axis in the figure has been re-scaled by the corresponding transition temperatures. We see that the peak in the entropy is much reduced compared to the previous calculations. The height of the peak is about a factor of two smaller compared to the previous calculations. Both larger quark masses and fewer quark flavors correspond to physical settings in between QCD with 2+1 flavors at physical quark masses and pure gauge theory. In pure gauge theory S_Q would diverge as the temperature approaches the deconfinement phase transition from above. We further remark that Fig. 6 clearly shows that the height of the peak decreases for increasing N_τ. Therefore, one would generally expect to see a higher peak in S_Q at finite cutoff than in the continuum limit. Hence, the much reduced height of the peak is no surprise.

Finally, let us discuss the behavior of S_Q in the high temperature region. For $T > 220$ MeV we have sufficiently accurate data for all lattice spacings. We have performed several continuum extrapolations based on global and local fits. These are shown in Fig. 8. We can see from the figure that different continuum extrapolations have overlapping error bands. In particular $N_\tau = 6$ data is consistent with $1/N_\tau^2$ scaling behavior. The uncertainty grows significantly, however, as we approach $T = 400$ MeV due to the fact that renormalization constants are available only up to that temperature for

[1] We adjusted for the change in the value of the kaon decay constant that was used to set the scale in Ref. [5] to the most recent value.

$N_\tau = 12$ data. In the next section we will discuss how to extend the results to higher temperatures. In Fig. 8 we also show the results for weak-coupling calculations at leading order with one-loop running coupling for two different renormalization scales. As one can see from the figure the LO result for S_Q is not very different from the lattice calculations, however, the scale dependence is quite large. Furthermore, higher order corrections are also important. Therefore, for a meaningful comparison of the lattice and the weak-coupling results it is necessary to extend the calculations to higher temperatures and to higher orders in the perturbative expansion. This will be discussed in section VII.

V. POLYAKOV LOOP AT HIGH TEMPERATURES

The highest temperature at which we can study the Polyakov loop or equivalently F_Q so far was limited by the knowledge of c_Q determined by the zero temperature static $Q\bar{Q}$ energy. Below we will discuss a method to work around this limitation which we call the direct renormalization scheme.

The idea of the direct renormalization scheme is to determine c_Q by comparing the free energy f_Q calculated for the same temperature but different N_τ [14]. Eq. (3) can be applied to obtain $c_Q(\beta)$ once $f_Q(T(\beta, N_\tau), N_\tau)$ and $f_Q^{\rm bare}(\beta, N_\tau)$ are known. If there were no cutoff effects in $f_Q(T(\beta, N_\tau), N_\tau)$ after renormalization, $c_Q(\beta)$ at some value of β would read

$$c_Q(\beta) = \frac{1}{N_\tau}\big[N_\tau^{\rm ref} c_Q(\beta^{\rm ref}) + f_Q^{\rm bare}(\beta^{\rm ref}, N_\tau^{\rm ref}) - f_Q^{\rm bare}(\beta, N_\tau)\big], \qquad (8)$$

where $N_\tau^{\rm ref}$ and $\beta^{\rm ref}$ correspond to a reference point, where c_Q is known.

Next, we study the cutoff dependence of f_Q. It is convenient to do so by considering the following difference

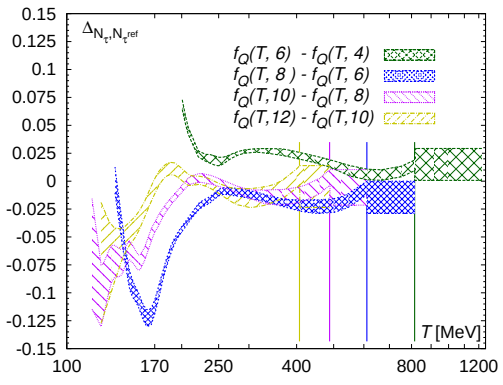

FIG. 9. (Color online) Extrapolation of residual cutoff effects in $f_Q^{\rm ren}(T(\beta, N_\tau), N_\tau^{\rm ref})$. The vertical lines indicate the start of the extrapolated $\Delta_{N_\tau,N_\tau^{\rm ref}}(T)$ for each pair $(N_\tau, N_\tau^{\rm ref})$.

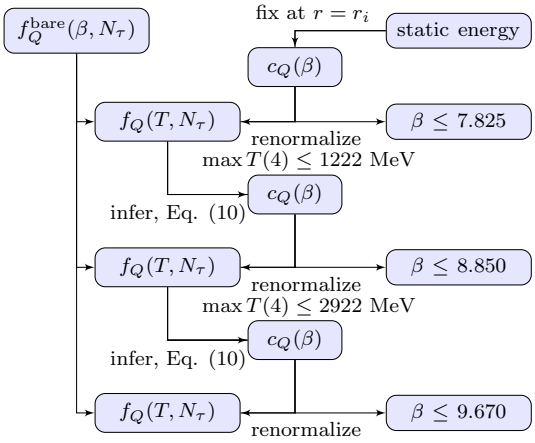

FIG. 10. (Color online) The flow chart sketches the different steps of the direct renormalization procedure. For each step the temperature $T(\beta, N_\tau)$ is limited by the corresponding $\beta \le \beta_{\rm max}$.

$$\Delta_{N_\tau,N_\tau^{\rm ref}}(T) = f_Q(T(\beta, N_\tau), N_\tau) - f_Q(T(\beta^{\rm ref}, N_\tau^{\rm ref}), N_\tau^{\rm ref}). \qquad (9)$$

In Fig. 9 we show $\Delta_{N_\tau,N_\tau^{\rm ref}}(T)$ as function of the temperature for different combinations of N_τ and $N_\tau^{\rm ref}$. At low temperatures, $T < 250$ MeV, this quantity shows a strong temperature dependence. However, for $T > 250$ MeV the temperature dependence of $\Delta_{N_\tau,N_\tau^{\rm ref}}(T)$ is rather mild, and one may approximate it by a constant. Therefore, we assume that above the temperatures where no lattice data for c_Q are available $\Delta_{N_\tau,N_\tau^{\rm ref}}(T)$ is constant. If predictions for c_Q from all possible pairs $(N_\tau, N_\tau^{\rm ref})$ are consistent within uncertainties, one may conclude in retrospect that the assumption was justified. We estimate its central value from the average of the minimum and the maximum of the one sigma band of $\Delta_{N_\tau,N_\tau^{\rm ref}}(T)$ for $T > 250$ MeV and its uncertainty by the respective difference. This estimate is shown in Fig. 9. Using $\Delta^{\rm av}_{N_\tau,N_\tau^{\rm ref}}(T)$ determined this way together with the corresponding error we can provide an estimate for c_Q that should be free of cutoff effects:

$$c_Q(\beta) = \frac{1}{N_\tau}\big[N_\tau^{\rm ref} c_Q^{Q\bar{Q}}(\beta^{\rm ref}) + \Delta^{\rm av}_{N_\tau,N_\tau^{\rm ref}} + f_Q^{\rm bare}(\beta^{\rm ref}, N_\tau^{\rm ref}) - f_Q^{\rm bare}(\beta, N_\tau)\big]. \qquad (10)$$

We use all possible pairs $(N_\tau, N_\tau^{\rm ref})$ and compute $c_Q^{\rm direct}(\beta, N_\tau, N_\tau^{\rm ref})$ via eq. (10) from $c_Q^{Q\bar{Q}}(\beta)$ for all possible temperatures. We can only calculate c_Q with direct renormalization procedure up to $\beta = 8.57$, if we use $N_\tau = 8$ results for the bare Polyakov loops ($T(\beta = 8.57, N_\tau = 8) = 1155$ MeV) or to $\beta = 8.85$ if we use $N_\tau = 12$ results for the bare Polyakov loop ($T(\beta = 8.85, N_\tau = 12) = 974$ MeV). To extend the beta range even further, we use

the two step procedure for the direct renormalization. First, we compute $c_Q^{\rm direct}$ up to $\beta = 8.85$ from $c_Q^{Q\bar{Q}}$ in the first iteration. Next, we add the new values of the renormalization constant to the bare free energies up to $T(\beta = 8.85, 4) = 2922$ MeV. Finally, we compute $c_Q^{\rm direct}$ up to $\beta = 9.67$ from $c_Q^{\rm direct}$ in a second iteration and add the new values of the renormalization constant to bare free energies up to $T(\beta = 9.67, 4) = 5814$ MeV. We sketch the procedure in the flow chart in Fig. 10. In order to test robustness and predictive power of direct renormalization, we omit $c_Q^{Q\bar{Q}}(\beta)$ for $\beta > 7.373$ and calculate $c_Q^{\rm direct}$ using the above procedure. After excluding $c_Q^{Q\bar{Q}}(7.596)$ and $c_Q^{Q\bar{Q}}(7.825)$ from the input, we compare the predictions for $c_Q^{\rm direct}(7.596, N_\tau, N_\tau^{\rm ref})$ and $c_Q^{\rm direct}(7.825, N_\tau, N_\tau^{\rm ref})$ with known values of $c_Q^{Q\bar{Q}}(\beta)$. We show this comparison for a few selected β values and pairs $(N_\tau, N_\tau^{\rm ref})$ in Fig. 11. Black bursts represent $c_Q^{Q\bar{Q}}(\beta)$ data from zero temperature lattices. Results $c_Q^{\rm direct}(\beta, N_\tau, N_\tau^{\rm ref})$ inferred from coarser resp. finer lattices ($N_\tau > N_\tau^{\rm ref}$ resp. $N_\tau < N_\tau^{\rm ref}$) are displaced to the right resp. left of $c_Q^{Q\bar{Q}}(\beta)$. Shape and color of the symbols encode $N_\tau^{\rm ref}$ and N_τ. As one can see from the figure the direct renormalization method correctly reproduces the values of the renormalization constant obtained in the $Q\bar{Q}$ procedure.

Since no trends in $c_Q^{\rm direct}(\beta, N_\tau, N_\tau^{\rm ref})$ depending on either N_τ or $N_\tau^{\rm ref}$ are observed, we conclude that no residual cutoff effects are present. We average over all possible pairs $(N_\tau, N_\tau^{\rm ref})$ that reproduce one of the β values of an underlying Polyakov loop within ± 0.01, take the error's mean as statistical error and the standard deviation as systematical error estimate (at most 25% of the statistical error). We add these errors in quadrature and show the 1σ bands of $c_Q^{\rm direct}(\beta)$ in the figure. We show with dark blue lines (for $\beta \leq 7.373$) that input values $c_Q^{Q\bar{Q}}(\beta)$

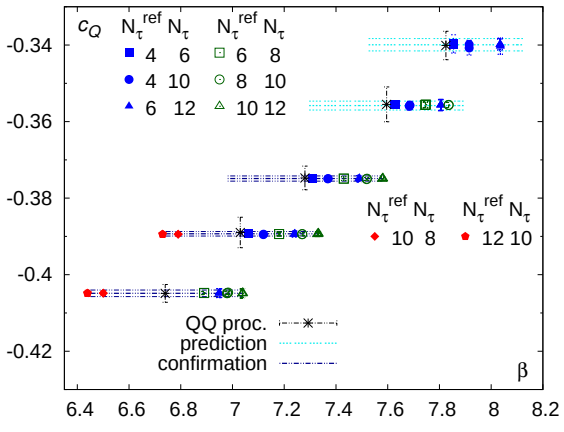

FIG. 11. (Color online) Comparison between renormalization constant $c_Q(\beta)$ from direct renormalization and $Q\bar{Q}$ procedures. Symbols and data are explained in the text.

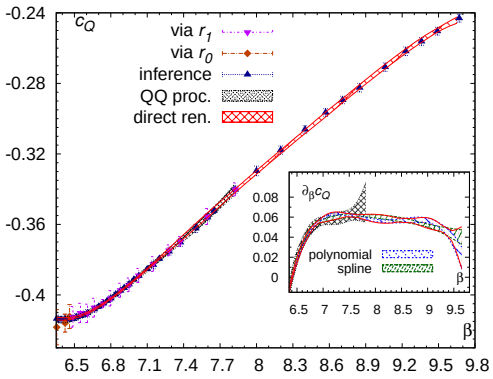

FIG. 12. (Color online) Renormalization constant $c_Q(\beta)$ from direct renormalization and $Q\bar{Q}$ procedures. Interpolations are shown as 1σ bands and data points are explained in the text. The inset shows the derivative $\frac{\partial c_Q}{\partial \beta}$.

are reproduced. Hence, consistency between both renormalization schemes is evident. We show with cyan lines (for $\beta > 7.373$) that predictions of the direct renormalization procedure are consistent with $c_Q^{Q\bar{Q}}(\beta)$ outside of the input β range. Therefore, we confirm that our approach for the direct renormalization procedure has predictive power outside of the input β range and that our extrapolation assuming constant cutoff effects in Fig. 9 is justified.

Having determined the renormalization constant in the extended range of β (cf. Fig. 12) it is straightforward to calculate the free energy f_Q at considerably higher temperatures. Namely our calculations with $N_\tau = 12$ now extend to $T = 900$ MeV, while for $N_\tau = 6$ and $N_\tau = 8$ we can reach to temperatures of about 3800 MeV and 2900 MeV, respectively. The results of our calculations at high temperatures ($T > 400$ MeV) are shown in Fig. 13 for different N_τ. In the figure we also show the local interpolation of the data as bands. One can see that the cutoff dependence of the data is rather mild, i.e. the bands corresponding to different N_τ are largely overlapping, including the $N_\tau = 4$ results. In other words, even for our coarsest lattice the cutoff effects are very small in this high temperature region. This will be important for the comparison with the weak-coupling calculations discussed in Section VII since this comparison can be performed using the $N_\tau = 4$ results that extend up to temperatures as high as 5814 MeV. We also note that the free energy becomes negative for $T > 500$ MeV as expected from the weak-coupling calculations. The other interesting feature of f_Q is that it has a minimum around temperatures of about 1500 MeV corresponding to a maximum of the renormalized Polyakov loop. This feature was observed in the SU(3) gauge theory, where the renormalized Polyakov loop has the maximum at temperatures of $12T_d$, with T_d being the deconfinement phase transition temperature [14]. These SU(3) Yang-Mills theory results, which have been included in Fig. 13, yield significantly smaller $|f_Q|$ than our results with 2+1 flavors. The dif-

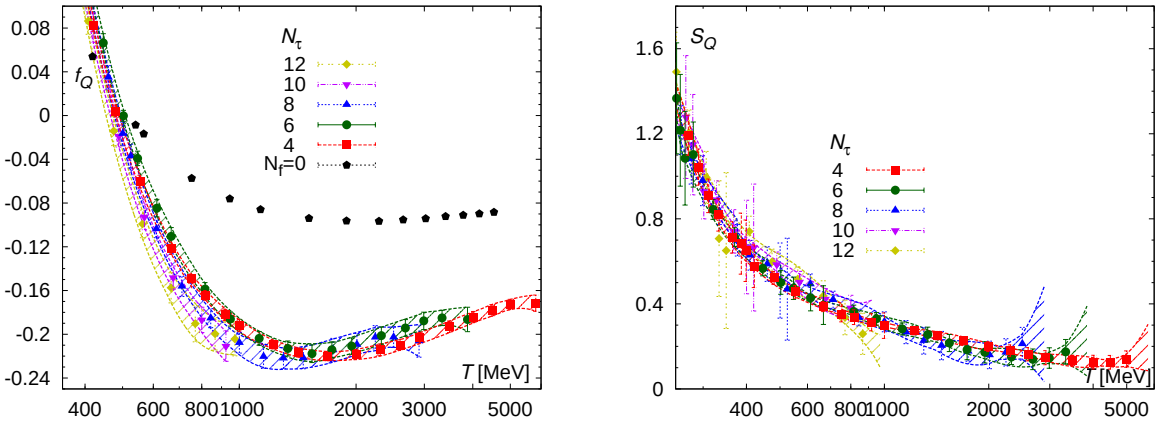

FIG. 13. (Color online) The free energy (left) and the entropy (right) of a static quark in the high temperature region. The bands show the results of interpolation with the corresponding uncertainty. For comparison, the free energy for SU(3) Yang-Mills theory on $N_\tau = 4$ lattices is included [14]. The dots on the right correspond to S_Q calculated from finite differences.

ference is pronounced most strongly in the vicinity of the minimum of f_Q.

From the interpolations of f_Q it is straightforward to calculate the entropy of a static quark. This is shown in Fig. 13 (right panel). Furthermore, since for $T > 400$ MeV the free energy varies smoothly with the temperature it is possible to calculate S_Q without any interpolation. We could estimate S_Q by approximating the temperature derivative of F_Q by finite differences of the lattice data on F_Q at two neighboring temperature values. The entropy estimated from the finite differences is also shown in Fig. 13 and it agrees very well with the results obtained from interpolations. For $T > 900$ MeV we have $S_Q \simeq -f_Q$ as expected in the weak-coupling picture. We also note that the entropy at high temperatures is also higher than in the SU(3) gauge theory.

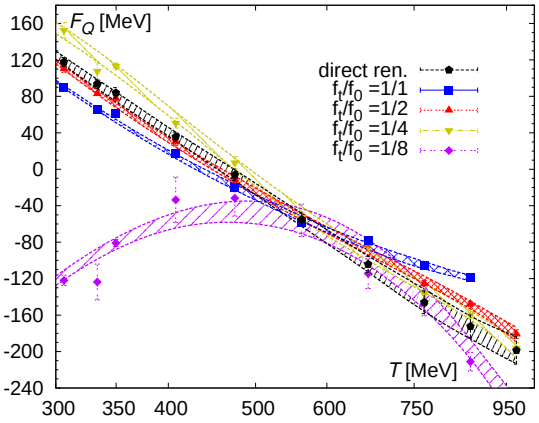

FIG. 14. (Color online) The free energy of a static quark calculated on $N_\tau = 12$ lattices for different flow times.

VI. RENORMALIZATION WITH GRADIENT FLOW

The gradient flow was introduced as a tool to remove short distance divergences in the lattice observables [44, 45]. It is defined by the differential equation [44]

$$\frac{dV_\mu(x,t)}{dt} = -g_0^2 \partial_{x,\mu} S[V] V_\mu(x,t), \qquad (11)$$

where $S[V]$ is the lattice gauge action and $g_0^2 = 10/\beta$ is the bare lattice gauge coupling. The new link variable $V_\mu(x,t)$ has the initial value given by the original link variable $V_\mu(x, t = 0) = U_\mu(x)$. Here we use the same notation for $\partial_{x,\mu} S[V]$ as in Ref. [44]. The gradient flow has been extensively used at zero temperature for scale setting (see, e.g., Ref. [46, 47]) as well as at non-zero temperature for the calculations of the equation of state [48]. In Ref. [49] it was proposed to use the gradient flow to calculate the renormalized Polyakov loops. It was shown there that up to a temperature independent

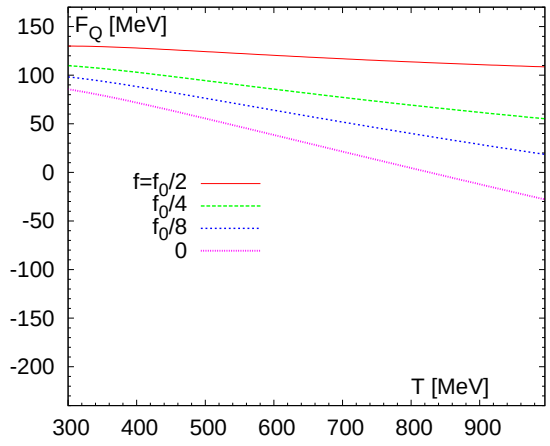

FIG. 15. (Color online) The free energy of a static quark at leading order calculated for different flow times. The values of the free energy have been shifted by 300 MeV (see text).

constant the free energy of a static quark calculated using the gradient flow agrees with the free energy obtained in the conventional ($Q\bar{Q}$) scheme in the continuum limit up to temperatures $T = 400$ MeV, provided that the flow time $f = \sqrt{8t}$ satisfies the condition:

$$a \ll f \ll 1/T, \quad \text{or} \quad 1 \ll fT \ll N_\tau. \tag{12}$$

The gradient flow method also enabled the calculation of the free energy of static charges in higher representation and confirmed the expected Casimir scaling in the high temperature region [49]. Here we would like to extend these studies to higher temperatures and also analyze the fluctuations of the Polyakov loop.

A. Renormalized Polyakov loop from gradient flow

We followed the procedure outlined in Ref. [49] and calculated the Polyakov loop at non-zero flow time by replacing the link variables $U_\mu(x)$ in Eq. (2) by $V_\mu(x,t)$. We use the tree level Symanzik gauge action in Eq. (11). We calculated the Polyakov loop for the same flow times as in Ref. [49], namely, $f = \sqrt{8t} = f_0,\ 3/4f_0, 1/2f_0, 1/4f_0$ and $1/8f_0$, $f_0 = 0.2129$ fm. See Ref. [49] for further details. In Fig. 14 we show our numerical results for $N_\tau = 12$ shifted by a constant such that the results obtained at different flow times agree with the continuum result for F_Q obtained in the previous section at $T = 600$ MeV. The bands shown in the figure correspond to the interpolation of the lattice data. One can see from the figure that the temperature dependence of F_Q obtained with $f = f_0,\ 3/4f_0, 1/2f_0$ is very similar to the temperature dependence of the free energy obtained using the direct renormalization procedure for $T < 500$ MeV. With a suitable constant shift all these results can be made to agree with each other in this temperature region. For higher temperatures, however, the temperature dependence of F_Q obtained with these values of the flow time is not captured correctly. Choosing a smaller flow time, namely $f = f_0/4$, the temperature dependence of F_Q obtained using direct renormalization method is reproduced. However, decreasing the flow time even further to $f_0/8$ leads to a completely different temperature dependence. Thus, for $T > 500$ MeV the results are very sensitive to the choice of the flow time, i.e. the scaling window is very narrow. We also performed the calculations for $N_\tau = 6,\ 8$ and 10. The corresponding results are similar to the ones shown in Fig. 14 but the flow time dependence is even stronger. This stronger flow time dependence is expected (cf. Eq. (12)).

To understand the flow time dependence of the free energy of a static quark shown in Fig. 14 it is useful to analyze the leading order result for the Polyakov loop obtained at non-zero flow time [50]. In terms of the free energy the leading order result reads

$$F_Q^f(T) = C_F\alpha_s\frac{\sqrt{\pi}}{f} - C_F\alpha_s\frac{m_D}{2}\tilde{\Phi}(m_D f/2), \tag{13}$$

where $\tilde{\Phi}(z) = e^{z^2}\frac{2}{\sqrt{\pi}}\int_z^\infty dx e^{-x^2}$. Here and in what follows we use the label f on the free energy to denote the free energy obtained with gradient flow. For sufficiently small flow time this result approaches the well known leading order result for F_Q (up to a temperature independent constant $\sim 1/f$), since $\tilde{\Phi}(z=0) = 1$. Now the question arises which value of the flow time can be considered as sufficiently small. Therefore, in Fig. 15 we show the leading order result given by Eq. (13) omitting the constant term $\sim 1/f$. Furthermore, we shifted F_Q^f by 300 MeV to facilitate the comparison with the lattice results. We see a similar trend in the flow time dependence of the leading order result for $F_Q^f(T)$: As the flow time increases the temperature dependence becomes milder. For $T < 400$ MeV $f = f_0/4$ can be considered as sufficiently small. However, at higher temperature we must have $f < f_0/8$. On the other hand, as we have seen above, the value of $f = f_0/8$ is too small for $N_\tau = 12$ lattices to remove the lattice artifacts. This suggests that one has to use lattices with temporal extent $N_\tau > 12$ to obtain the correct temperature dependence of the Polyakov loop for $T > 400$ MeV.

One could also try to follow a different philosophy and fix the flow time such that $f \cdot T = const.$ as it was done in Ref. [50]. In this case the term proportional to $1/f$ would contribute to the temperature dependence of F_Q^f and thus to the entropy $S_Q^f = -\partial F_Q^f/\partial T$. The additional contribution to the entropy just amounts to a constant shift compared to the entropy of a static charge defined in the conventional way, i.e. the temperature dependence of the entropy would be the same as before. By matching the entropy obtained from the gradient flow to the entropy of a static quark obtained in the conventional scheme one could in principle obtain results for the entropy at higher temperatures. We tried to implement this scheme, however, it turns out that the resulting errors are too large to obtain reliable results for the entropy of a static charge at high temperatures.

B. Fluctuations of Polyakov loop

The Polyakov loop susceptibility defined as

$$\chi = (VT^3)\left(\langle|P|^2\rangle - \langle|P|\rangle^2\right), \tag{14}$$

is often used to study the deconfinement transition in SU(N) gauge theories and for the determination of the transition temperature. It has a sharp peak at the pseudo-critical temperature. It is not clear, however, how to renormalize this quantity. Attempts to renormalize it using the square of the renormalization factor of the Polyakov loop have been proposed [32, 51]. However, apart from being ad-hoc this procedure does not remove all the UV divergences in the susceptibility as can be seen from the comparison of lattice data obtained for different N_τ [32]. In Ref. [50] the gradient flow was used in the

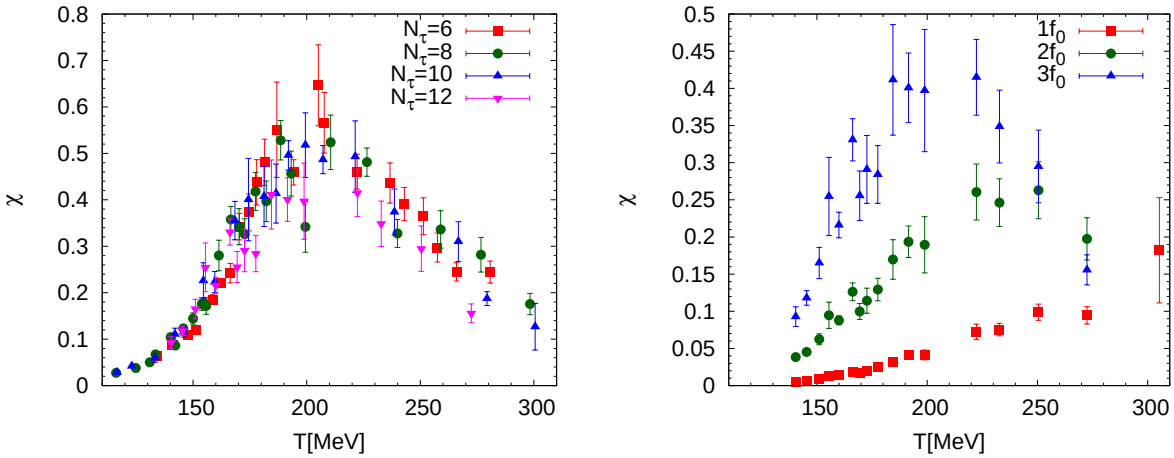

FIG. 16. (Color online) The Polyakov loop susceptibility obtained using gradient flow for $f = 3f_0$ and different N_τ (left) and for $N_\tau = 12$ and $f = f_0, 2f_0$ and $3f_0$.

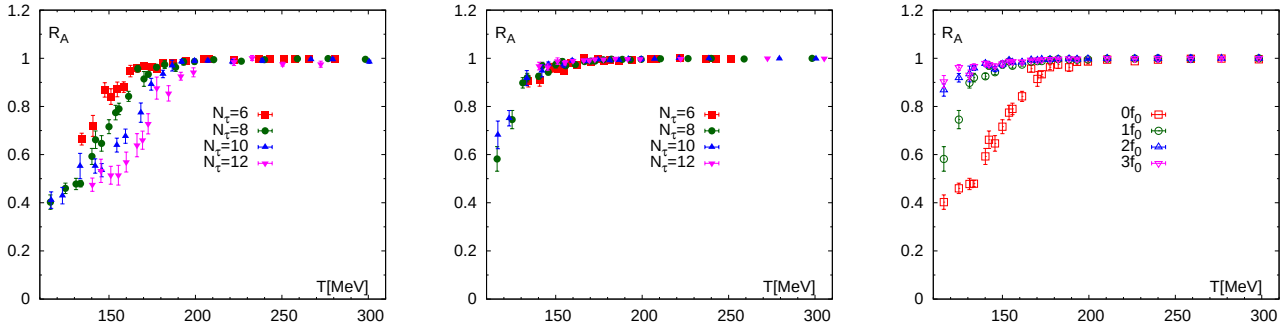

FIG. 17. (Color online) The ratio of the susceptibilities R_A shown as function of the temperature for zero flow time (left), flow time $f = f_0$ (middle) and for different flow times but for $N_\tau = 8$ (right).

calculation of the Polyakov loop susceptibilities in SU(3) gauge theory. The gradient flow effectively renormalizes the susceptibility and thus no cutoff dependence can be seen [50], but the value of the Polyakov susceptibility depends on the choice of the flow time. The peak position is, however, independent of the flow time and is equal to the phase transition temperature [50].

We also used gradient flow to study the Polyakov loop susceptibility in 2+1 flavor QCD. Our results for flow time $f = 3f_0$ and different N_τ are shown in Fig. 16 (left panel). The Polyakov loop susceptibility obtained for $f = 3f_0$ shows a peak around $T \simeq 200$ MeV, i.e. at significantly higher temperature than T_c (e.g. $T_S(N_\tau = 12) = 157(6)\,\mathrm{MeV}$). The N_τ dependence of the Polyakov loop is rather mild and does not show a clear tendency. Next, we examine the dependence of the Polyakov loop susceptibility on the flow time. In Fig. 16 (right panel) we also show the flow time dependence of χ for $N_\tau = 12$, where the flow time dependence is expected to be the mildest. We see that the Polyakov loop susceptibility strongly depends on the choice of the flow time. The peak position shifts to large values as the flow time is decreased from $3f_0$ to f_0. This behavior of the Polyakov loop susceptibility in 2+1 flavor QCD can be understood as follows. Unlike in SU(N) gauge theory the Polyakov loop is not related to singular behavior of the free energy in the transition region. The fluctuations of the Polyakov loop are therefore not affected by the critical behavior in the transition region and thus are not enhanced in a significant way. The value of χ is determined by the regular terms and thus depends on the renormalization procedure, i.e., the choice of the flow time.

In addition to the Polyakov loop susceptibility defined by Eq. (14), which corresponds to the fluctuation in the absolute value of the Polyakov loop, one can consider separately the fluctuations of real and imaginary parts of the Polyakov loop

$$\chi_L = (VT)^3\langle(\mathrm{Re}P)^2\rangle - \langle P\rangle^2, \quad \chi_T = (VT)^3\langle(\mathrm{Im}P)^2\rangle, \tag{15}$$

which, following Refs. [32, 51], we will call the longitudinal and transverse susceptibilities. In the above equations we used the fact that $\langle P\rangle = \langle \mathrm{Re}P\rangle$ and $\langle \mathrm{Im}P\rangle = 0$. We have calculated χ_L and χ_T using the gradient flow. We find that χ_L behaves as χ, i.e. it has the same flow time dependence, and for $f = 3f_0$ it shows a broad peak

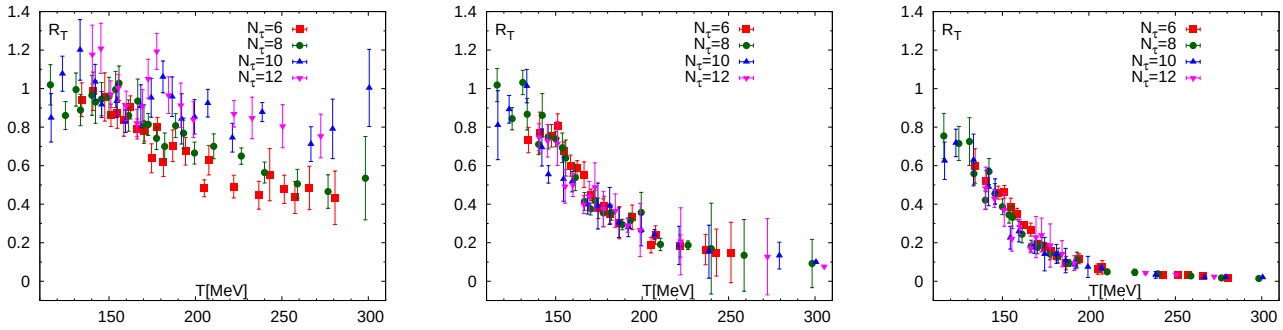

FIG. 18. (Color online) The ratio of the susceptibilities R_T shown as function of the temperature for zero flow time (left), flow time $f = f_0$ (middle) and for flow time $f = 3f_0$ (right).

in the temperature region $T = (180 - 200)$ MeV. We also find a significant flow time dependence for χ_T. However, χ_T has a peak at temperatures around 160 MeV, i.e. close to the chiral transition temperature. One may speculate that with increasing the flow time further the peak position of χ_L will move closer to the chiral transition temperature because the large flow time will enhance the infrared fluctuations in the real part of the Polyakov loop. However, we did not pursue this in the present study.

In Refs. [32, 51] the ratios of the Polyakov loop susceptibilities $R_A = \chi/\chi_L$ and $R_T = \chi_T/\chi_L$ have been studied. It has been argued there that these ratios are sensitive probes of deconfinement and are independent of the cutoff. Therefore, we will study these ratios in more detail. First, let us consider the ratio R_A. It is shown in Fig. 17 as function of the temperature for various flow times and lattice spacings. For zero flow time our results for R_A are in qualitative agreement with the results of Ref. [32]. The ratio R_A exhibits a crossover behavior for temperatures $T = (150 - 200)$ MeV. However, we see a very strong cutoff (N_τ) dependence of this ratio. While for $N_\tau = 8$ the crossover happens at temperatures close to the chiral transition temperatures, for larger N_τ it happens at significantly higher temperatures. For flow time $f = f_0$ we do not see any significant cutoff dependence in R_A, i.e. this value of the flow time is sufficiently large to get rid of the cutoff effects and obtain a renormalized quantity for R_A (cf. the middle panel of Fig. 17). Since cutoff effects are quite small already for $f = f_0$ it is sufficient to study the flow time dependence of our results for the $N_\tau = 8$ lattice data, which is also shown in Fig. 17. One can see from the figure that as the flow time increases the value of R_A at low temperatures increases, and the step function like behavior of R_A gradually disappears. For flow time $f = 2f_0$ and $f = 3f_0$ the ratio R_A smoothly approaches one from below as the temperature increases and shows no sign of an inflection point. Note, that there is no significant flow time dependence for $f \geq 2f_0$ in R_A. The flow time dependence for other N_τ is similar.

Now let us examine the temperature dependence of R_T. In Fig. 18 we show our results for R_T for three different flow times: $f = 0, f_0$ and $3f_0$. For zero flow time we see sizable cutoff dependence in R_T and our results are qualitatively similar to those of Ref. [32]. For flow time $f = f_0$ the large cutoff dependence is removed and we see a crossover like behavior around temperatures of about 160 MeV. For $f = 3f_0$ we have a very similar picture and again we see a crossover behavior around temperatures of about 160 MeV. However, the value of R_T is somewhat reduced at low temperatures.

In summary, we find that the ratios R_A and R_T are strongly cutoff dependent contrary to the conjecture of Refs. [32, 51] stating their cutoff independence. Evaluating these ratio with the gradient flow removes the cutoff dependence. However, R_A obtained from the gradient flow is not sensitive to deconfinement. On the other hand R_T obtained from the gradient flow is sensitive to deconfinement, it shows a crossover behavior close to the chiral crossover temperature. Furthermore, R_T is not very sensitive to the choice of the flow time, and therefore it can be considered as a sensitive probe of deconfinement.

VII. COMPARISON WITH THE WEAK-COUPLING CALCULATIONS

In this section we discuss the comparison of our lattice results with the weak-coupling calculations. The free energy of a static quark has been calculated to next-to-next-to leading order (NNLO) [17]. It is important to calculate the free energy to this order to reduce the large scale dependence of the weak-coupling result. We will use the $N_\tau = 4$ results for this comparison as these extend up to the rather high temperatures of 5814 MeV and the lattice artifacts are small, see discussions in Section V. As was pointed out in Ref. [17] the comparison of the lattice results and the weak-coupling calculations is complicated by the fact that the two calculations are performed in different schemes. The weak-coupling calculations are performed in $\overline{MS}$ scheme, while in the lattice calculations the scheme is fixed by the prescribed values of the static $Q\bar{Q}$ energy at zero temperature at some distance. The

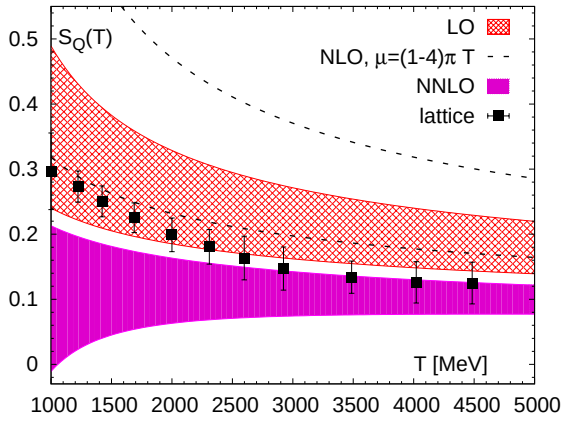

FIG. 19. (Color online) The lattice results obtained with $N_\tau = 4$ compared to the weak-coupling calculations.

two schemes can be related by a constant (temperature independent) shift in F_Q that can be calculated. This, however, introduces additional uncertainty in the comparison. The most straightforward way to perform the comparison of the lattice and the weak-coupling results is to consider the entropy [17]. Such a comparison has been performed in SU(3) gauge theory, i.e. for $N_f = 0$ in a temperature range extending up to $24T_d$, with $T_d \simeq 300$ MeV being the deconfinement phase transition temperature in [17]. It was found that the lattice data are in between the leading order (LO) and the NNLO results, and at the highest temperature the NNLO and the lattice results agree within the uncertainties.

In Fig. 19 we show the comparison of the LO and NNLO weak-coupling results with the $N_\tau = 4$ results for S_Q. We used the 1-loop running coupling constant in the weak-coupling calculations and the value $\Lambda_{\overline{MS}} = 315$ MeV obtained from the static energy at zero temperature [52]. This value is compatible with the earlier determination from the static energy in Ref. [53]. The bands shown in Fig. 19 correspond to scale variations between $\mu = \pi T$ and $\mu = 4\pi T$. At the highest temperature the lattice results and the NNLO results agree within the estimated uncertainties. At lower temperatures, $T < 1500$ MeV the lattice results are closer to the LO weak-coupling results. For $T < 1000$ MeV the NNLO result for S_Q can turn negative for some choices of the renormalization scale. This is clearly an unphysical behavior indicating that higher-order corrections are too large. The situation is quite different from the case of quark number susceptibilities, where the weak-coupling prediction seems to work for $T > 300$ MeV [35, 36]. This is due to the fact that quark number susceptibilities are dominated by the contribution of the non-static Matsubara modes, while for the free energy of a static quark the dominant contribution comes from the static sector [17]. Overall, the agreement of the weak-coupling and the lattice results for S_Q is similar to the case of the SU(3) gauge theory. As previously noted in section V the value of S_Q at high temperature in QCD is larger than in the SU(3) gauge theory. This increase is well explained by the weak-coupling calculations.

VIII. CONCLUSIONS

In summary, we have calculated the free energy of a static quark in 2+1 flavor QCD at physical quark masses using several lattice spacings and in a large temperature range. We have presented continuum results for this quantity at much higher temperature than previously available. We also calculated the entropy of a static quark and showed that it is a useful quantity for studying deconfinement in 2+1 flavor QCD. Namely, we showed that it has a peak at a temperature around the chiral transition temperature, indicating that deconfinement and chiral transitions happen at similar temperatures. The entropy of a static quark is also useful for comparing lattice and weak-coupling results at high temperatures. Since the cutoff effects are very small at high temperatures we could do this comparison using the $N_\tau = 4$ lattice results which extend up to temperatures as high as 5814 MeV. At the highest temperatures we see agreement between the lattice and the NNLO weak-coupling results within the estimated uncertainties but at lower temperatures higher-order corrections become large and the weak-coupling expansion may not be reliable.

We also studied the fluctuations of the Polyakov loop using the gradient flow. We showed that Polyakov loop susceptibilities can be renormalized using the gradient flow and the transverse Polyakov loop susceptibility may be a sensitive probe of deconfinement.

ACKNOWLEDGMENTS

This work was supported by U.S. Department of Energy under Contract No. DE-SC0012704. We acknowledge the support by the DFG Cluster of Excellence "Origin and Structure of the Universe" (Universe cluster). The calculations have been carried out on Blue Gene/L computer of New York Center for computational Science in BNL, at NERSC, on the computing facilities of the Computational Center for Particle and Astrophysics (C2PAP) and on SuperMUC cluster of the Leibniz Supercomputer Center (LRZ). Usage of C2PAP and SuperMUC took place under the three Universe cluster grants "Static Quark Correlators in lattice QCD at nonzero temperature" for 2014, 2015 and 2016 (project ID pr83pu) and the LRZ grant "Properties of QCD at finite temperature" for 2015 (project ID pr48le). N. Brambilla, A. Vairo and J. H. Weber acknowledge the support by the Universe cluster for the seed project "Simulating the Hot Universe", by the Bundesministerium für Bildung und Forschung (BMBF) under grant "Verbundprojekt 05P2015 - ALICE at High Rate (BMBF-FSP 202) GEM-TPC Upgrade and Field theory based investiga-

tions of ALICE physics" under grant No. 05P15WOCA1 and by the Kompetenznetzwerk für Wissenschaftliches Höchstleistungsrechnen in Bayern (KONWIHR) for the Multicore-Software-Initiative with the project "Production of gauge configurations at zero and non-zero temperature" (KONWIHR-IV). H.-P. Schadler was funded by the FWF DK W1203 "Hadrons in Vacuum, Nuclei and Stars".

Appendix A: Details of the lattice calculations

In this appendix we will discuss the gauge configurations and the calculation of the bare Polyakov loop used in the present analysis as well as some other details of the lattice calculations. As mentioned in Section II we have used the gauge configurations and the bare Polyakov loop calculated by the HotQCD Collaboration in Refs. [24, 34]. The parameters corresponding to these gauge configurations, including the gauge coupling β, strange quark mass and the accumulated statistics are given in Table VI of Ref. [24] and Table III of Ref. [34]. The values of the bare Polyakov loops are given in Tables X, XI and XII of Ref. [24] and Tables IX, X, XI and XII of Ref. [34]. We also used the Polyakov loop calculated on $40^3 \times 10$ lattices in Ref. [25]. To extend the calculations of the Polyakov loop to significantly higher temperatures we performed calculations on $16^3 \times 4$ lattices. The parameters of these calculations along with the expectation values of the bare Polyakov loop are given in Table III. We also used the gauge configurations generated for the study of the quark number susceptibilities in Refs. [35, 36]. The bare lattice parameters and the statistics corresponding to these gauge configurations are given in Table II. We extended the beta range for $N_\tau = 6,\ 8$ and these additional ensembles are also shown in Table II. The expectation values of the bare Polyakov loop are also shown in this Table. Finally, we have found it necessary to extend some of the previous gauge ensembles in order to have sufficiently small error for $L^{\rm bare}$. These ensembles with extended statistics are given in Table I. We further added a few new gauge ensembles with low beta for $N_\tau = 12$, which are also included in the same Table. Since we found for some ensembles with relatively small ensemble sizes that Jackknife errors are disproportionally small compared to ensembles with much larger ensemble sizes, we enlarged the respective Jackknife errors by a factor two. This set of ensembles with manually enlarged errors consists of $\beta = 6.195$, 6.245, 6.260, 6.285, 6.315, 6.341 and 6.445 for $N_\tau = 8$ and $\beta = 6.990$, 7.100 and 7.200 for $N_\tau = 12$. The criteria for enlarging the Jackknife errors for $N_\tau = 8$ respectively 12 was statistics with less than 60000 TU respectively 10000 TU. Since we did not modify the central values, these data may have a particularly adverse effect for the calculation of the entropy in the respective temperature ranges.

In Table IV we give the values of the renormalization constant c_Q obtained from the static energy at zero temperature. The renormalization constants corresponding to the direct renormalization are listed in Table V.

β	am_s	N_τ	#TU	$L^{\rm bare}$
6.2850	0.079000	10	9260	0.000200(15)
6.3410	0.074000	10	39220	0.000256(08)
6.4230	0.067000	10	10350	0.000403(12)
6.4450	0.065200	8	19150	0.004353(41)
6.5150	0.060400	12	32510	0.000121(13)
6.6080	0.054200	12	19890	0.000198(07)
6.6640	0.051400	12	29590	0.000295(07)
6.7000	0.049600	12	17070	0.000369(08)
6.7700	0.046000	12	16890	0.000585(11)
6.8400	0.043000	12	18720	0.000930(14)
6.9100	0.040000	12	9230	0.001382(18)

TABLE I. List of extended and new gauge ensembles and the corresponding parameters.

We used the gradient flow to calculate the renormalized Polyakov loop expectation value and the Polyakov loop susceptibilities. We always used step size $dt = 0.01$ in lattice units in our gradient flow study. The parameters of the gradient flow analysis, including the values of β, the number of gauge configurations analyzed and the maximal flow time $t_{\rm max}$ are given in Tables VI, VII, VIII and IX.

Appendix B: Interpolations and extrapolations

In this appendix we present some details of our interpolation procedure. As discussed in the main text we use polynomial fits and smoothing splines for the interpolations. The calculations of c_Q and the corresponding interpolations are performed in three steps. In the first step we interpolate the value of c_Q obtained in the $Q\bar{Q}$ procedure in the interval $\beta = 5.900 - 7.825$. Then we use c_Q obtained in the direct renormalization procedure and interpolate in the interval $\beta = 5.900 - 8.850$. Finally we calculate c_Q at higher β using direct renormalization only and interpolate in the interval $\beta = 5.900 - 9.67$. The details of the interpolations are given in Table X. In the Table, n_k is the number of knots for spline interpolations and sm is the smoothing parameter for the built-in smooth spline interpolations of the R statistical package [54]. n_p is the polynomial order for polynomial interpolations. We refer to the interpolation of c_Q from $Q\bar{Q}$ procedure as the 0th iteration of direct renormalization.

To calculate the entropy we also perform interpolations of the bare free energy in β. The details of these interpolations are presented in Table XI. The column labels are the same as in Table X.

In some temperature ranges, continuum extrapolations do not converge well and yield $\chi^2/{\rm df} > 1$. Firstly, in the temperature interval 176 MeV $< T <$ 189 MeV, local

β	am_s	$N_\tau = 12$		$N_\tau = 10$		$N_\tau = 8$		$N_\tau = 6$	
		#TU	$L^{\rm bare}$	# TU	$L^{\rm bare}$	#TU	$L^{\rm bare}$	#TU	$L^{\rm bare}$
7.2000	0.029600	4590	0.004236(34)	4990	0.013329(77)	—	—	—	—
7.5000	0.022200	8990	0.008988(35)	4990	0.022541(89)	4990	0.053915(132)	6670	0.125003(202)
7.6500	0.019200	6220	0.011604(79)	2990	0.027463(107)	2990	0.062378(213)	—	—
8.0000	0.014000	6090	0.019224(89)	39270	0.040274(211)	21810	0.083107(317)	4200	0.165828(296)
8.2000	0.011670	30090	0.024071(46)	27490	0.047833(97)	3070	0.093920(224)	10110	0.181014(126)
8.4000	0.009750	29190	0.029292(53)	8530	0.055774(114)	2990	0.105302(286)	10160	0.195736(153)
8.5700	0.008376	3040	0.033996(136)	2990	0.062941(191)	10260	0.115224(140)	10200	0.208437(141)
8.7100	0.007394	3140	0.037736(117)	–	–	10040	0.122951(148)	10230	0.217793(125)
8.8500	0.006528	2990	0.041652(169)	–	–	10010	0.130870(126)	10070	0.227509(159)
9.060	0.004834	–	–	—	—	10820	0.142401(130)	10080	0.241385(124)
9.230	0.004148	–	–	—	—	10260	0.152031(119)	10070	0.252699(154)
9.360	0.003691	–	–	—	—	8130	0.158728(172)	8250	0.260614(197)
9.490	0.003285	–	–	—	—	8020	0.165972(115)	8140	0.268749(158)
9.670	0.002798	–	–	—	—	8060	0.174995(146)	10300	0.279328(173)

TABLE II. The parameters and the expectation values of the bare Polyakov loops for the high temperature runs for $N_\tau = 6,\ 8,\ 10$ and 12.

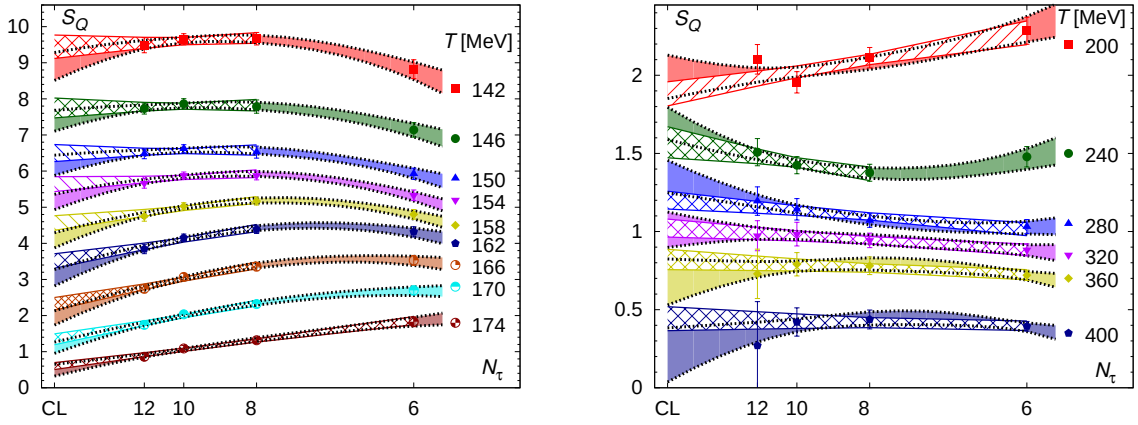

FIG. 20. (Color online) The static quark entropy at various temperatures as function of $1/N_\tau^2$. 'CL' marks the continuum limit ($N_\tau \to \infty$). The $1/N_\tau^2$ continuum extrapolations are shown as bands with filled pattern. The continuum extrapolations with $1/N_\tau^4$ term included are shown as solid filled bands. The widths of the band shows the statistical uncertainty of the fits. The left panel shows the results in the low temperature region, while the right panel shows the result in the high temperature region.

continuum extrapolations of F_Q with $N_\tau \geq 8$ yield up to $\chi^2/\mathrm{df} = 1.23$ (cf. Fig. 3). Secondly, in the temperature interval 150 MeV $< T <$ 169 MeV, local continuum extrapolations of S_Q yield up to $\chi^2/\mathrm{df} = 1.50$ with $N_\tau \geq 8$ and $c = 0$. Thirdly, in the temperature interval 190 MeV $< T <$ 211 MeV, local continuum extrapolations of S_Q yield up to $\chi^2/\mathrm{df} = 3.37$ with $N_\tau \geq 6$ and $c \neq 0$ and up to $\chi^2/\mathrm{df} = 3.69$ with $N_\tau \geq 8$ and $c = 0$. Judging from Fig. 20, these poor continuum extrapolations are caused by fluctuations of some $N_\tau = 12$ data in the interval 190 MeV $< T <$ 211 MeV, which originate in the relatively small ensemble sizes underlying some data in this interval (cf. Appendix A).

We summarize the global fits in Table XII. Hereby, $n_i,\ i = 0, 2, 4$ are the orders of the temperature polynomials $P_i(T)$ as in Eq. (4). We include in the table ratios $R[N_\tau] = \chi^2[N_\tau]/n_{\rm pt}[N_\tau]$ as measure how well data for each N_τ is matched by the global fit. Global residuals of $\chi^2/\mathrm{df} \lesssim 0.3$ are required to bring all ratios $R[N_\tau]$ sufficiently below one such that global fits yield reliable results.

We collect the final, continuum extrapolated results for the free energy and entropy in Table XIII.

β	am_s	T [MeV]	#TU	$L^{\rm bare}$
5.900	0.132000	201	65350	0.05906(11)
6.000	0.113800	221	62610	0.07475(15)
6.050	0.106400	232	62400	0.08280(13)
6.125	0.096600	249	63510	0.09502(17)
6.215	0.086200	272	26650	0.10985(21)
6.285	0.079000	291	25380	0.12144(16)
6.354	0.072800	311	19480	0.13242(15)
6.423	0.067000	333	21930	0.14331(17)
6.515	0.060300	364	31330	0.15767(14)
6.575	0.056400	386	22770	0.16674(12)
6.608	0.054200	399	39400	0.17192(12)
6.664	0.051400	421	75770	0.17996(09)
6.800	0.044800	480	37860	0.19956(10)
6.950	0.038600	554	38090	0.21979(11)
7.150	0.032000	669	31800	0.24452(12)
7.280	0.028400	753	42810	0.25964(10)
7.373	0.025000	819	65010	0.26990(10)
7.500	0.022200	918	42950	0.28351(10)
7.596	0.020200	1000	69920	0.29314(10)
7.825	0.016400	1222	65380	0.31535(08)
8.000	0.014000	1422	27510	0.33112(11)
8.200	0.011670	1687	20790	0.34806(13)
8.400	0.009750	1999	20950	0.36397(18)
8.570	0.008376	2308	20280	0.37672(08)
8.710	0.007394	2597	20200	0.38712(10)
8.850	0.006528	2921	19210	0.39680(11)
9.060	0.004834	3487	20950	0.41113(07)
9.230	0.004148	4021	21240	0.42222(08)
9.360	0.003691	4484	10620	0.43025(14)
9.490	0.003285	5000	10320	0.43755(15)
9.670	0.002798	5814	10340	0.44799(15)

TABLE III. The parameters of $N_\tau = 4$ ensembles and the corresponding expectation values of the bare Polyakov loops.

β	c_Q	β	c_Q	β	c_Q
5.9000	-0.3773(39)	6.4230	-0.4160(41)	6.8800	-0.3973(29)
6.0000	-0.3914(66)	6.4600	-0.4122(55)	6.9500	-0.3943(28)
6.0500	-0.3983(64)	6.4880	-0.4124(44)	7.0300	-0.3890(29)
6.1000	-0.3993(58)	6.5500	-0.4102(41)	7.1500	-0.3824(30)
6.1950	-0.4092(60)	6.6080	-0.4105(39)	7.2800	-0.3747(23)
6.2850	-0.4103(65)	6.6640	-0.4072(39)	7.3730	-0.3696(19)
6.3410	-0.4152(24)	6.7400	-0.4049(17)	7.5960	-0.3555(32)
6.3540	-0.4183(81)	6.8000	-0.4019(32)	7.8250	-0.3401(26)

TABLE IV. The renormalization constant c_Q is obtained from the static energy at zero temperature.

β	c_Q	β	c_Q	β	c_Q
5.9000	-0.3788(25)	6.4450	-0.4139(10)	7.1500	-0.3830(22)
5.9500	-0.3853(23)	6.4600	-0.4138(14)	7.2000	-0.3795(08)
6.0000	-0.3917(18)	6.4880	-0.4135(11)	7.2800	-0.3754(20)
6.0250	-0.3942(16)	6.5150	-0.4125(19)	7.3730	-0.3702(23)
6.0500	-0.3973(20)	6.5500	-0.4120(11)	7.5000	-0.3623(23)
6.0750	-0.3994(16)	6.5750	-0.4112(13)	7.5960	-0.3560(20)
6.1000	-0.4012(29)	6.6080	-0.4103(20)	7.6500	-0.3523(14)
6.1250	-0.4041(22)	6.6640	-0.4081(17)	7.8250	-0.3403(21)
6.1500	-0.4052(15)	6.7000	-0.4067(10)	8.0000	-0.3297(27)
6.1750	-0.4069(18)	6.7400	-0.4048(08)	8.2000	-0.3179(23)
6.1950	-0.4084(22)	6.7700	-0.4034(08)	8.4000	-0.3062(21)
6.2150	-0.4091(16)	6.8000	-0.4019(15)	8.5700	-0.2965(22)
6.2450	-0.4111(16)	6.8400	-0.3996(11)	8.7100	-0.2894(21)
6.2600	-0.4116(16)	6.8800	-0.3976(07)	8.8500	-0.2825(24)
6.2850	-0.4120(20)	6.9100	-0.3961(06)	9.0600	-0.2708(24)
6.3150	-0.4134(13)	6.9500	-0.3940(16)	9.2300	-0.2618(24)
6.3540	-0.4135(20)	6.9900	-0.3913(07)	9.3600	-0.2562(22)
6.3900	-0.4140(18)	7.0300	-0.3892(08)	9.4900	-0.2504(22)
6.4230	-0.4136(24)	7.1000	-0.3854(07)	9.6700	-0.2431(22)

TABLE V. The renormalization constant c_Q from the direct renormalization procedure.

[1] A. Bazavov, PoS **LATTICE2014**, 392 (2015).
[2] H.-T. Ding, F. Karsch, and S. Mukherjee (2015), 1504.05274.
[3] P. Petreczky, J. Phys. **G39**, 093002 (2012), 1203.5320.
[4] G. Boyd, J. Engels, F. Karsch, E. Laermann, C. Legeland, M. Lutgemeier, and B. Petersson, Nucl. Phys. **B469**, 419 (1996), hep-lat/9602007.
[5] Y. Aoki, G. Endrodi, Z. Fodor, S. D. Katz, and K. K. Szabo, Nature **443**, 675 (2006), hep-lat/0611014.
[6] A. Bazavov, H. T. Ding, P. Hegde, O. Kaczmarek, F. Karsch, *et al.*, Phys. Rev. Lett. 111, **111**, 082301 (2013), 1304.7220.
[7] A. Bazavov, H.-T. Ding, P. Hegde, O. Kaczmarek, F. Karsch, *et al.*, Phys.Lett. **B737**, 210 (2014), 1404.4043.
[8] R. Bellwied, S. Borsanyi, Z. Fodor, S. D. Katz, and C. Ratti, Phys.Rev.Lett. **111**, 202302 (2013), 1305.6297.
[9] S. Mukherjee, P. Petreczky, and S. Sharma, Phys. Rev. **D93**, 014502 (2016), 1509.08887.
[10] L. D. McLerran and B. Svetitsky, Phys. Rev. **D24**, 450 (1981).
[11] O. Kaczmarek, F. Karsch, P. Petreczky, and F. Zantow, Phys. Lett. **B543**, 41 (2002), hep-lat/0207002.
[12] S. Digal, S. Fortunato, and P. Petreczky, Phys. Rev. **D68**, 034008 (2003), hep-lat/0304017.
[13] O. Kaczmarek, F. Karsch, F. Zantow, and P. Petreczky, Phys. Rev. **D70**, 074505 (2004), [Erratum: Phys. Rev.D72,059903(2005)], hep-lat/0406036.
[14] S. Gupta, K. Huebner, and O. Kaczmarek, Phys. Rev. **D77**, 034503 (2008), 0711.2251.

β	$t_{\max}$	# TU	β	$t_{\max}$	# TU
5.850	0.850	5000	6.354	2.150	5000
5.900	0.900	5000	6.423	2.400	5000
5.950	1.000	5000	6.488	2.750	5000
6.000	1.100	5000	6.515	2.900	5000
6.025	1.150	5000	6.550	3.100	5000
6.050	1.200	5000	6.575	3.250	5000
6.075	1.250	5000	6.608	3.450	5000
6.100	1.300	5000	6.664	3.800	5000
6.125	1.350	5000	6.800	4.900	5000
6.150	1.450	5000	6.950	6.500	5000
6.175	1.500	5000	7.150	1.100	5000
6.195	1.550	5000	7.280	1.400	1000
6.215	1.700	5000	7.373	1.650	1000
6.245	1.700	5000	7.500	2.050	1000
6.285	1.850	5000	7.596	2.400	1000
6.341	2.050	5000	7.825	3.550	1000

TABLE VI. $24^3 \times 6$ gauge configurations used for the gradient flow analysis.

β	$t_{\max}$	# TU	β	$t_{\max}$	# TU
6.285	1.850	2420	6.950	6.500	5000
6.341	2.050	5000	7.030	7.550	5000
6.423	2.450	3640	7.150	9.450	5000
6.488	2.700	5000	7.200	11.500	1000
6.515	2.850	5000	7.280	12.000	1000
6.575	3.200	5000	7.373	1.600	1000
6.608	3.400	5000	7.500	2.100	4000
6.664	3.800	5000	7.596	2.400	1000
6.700	4.050	4000	7.650	2.650	1000
6.740	4.400	5000	7.825	3.500	1000
6.770	4.650	4460	8.000	4.800	1000
6.800	4.900	5000	8.200	6.700	1000
6.840	5.300	4580	8.400	9.400	1000
6.880	5.700	9720	8.570	12.500	1000

TABLE VIII. $40^3 \times 10$ gauge configurations used for the flow analysis.

β	$t_{\max}$	# TU	β	$t_{\max}$	# TU
6.050	1.200	5000	6.575	3.200	5000
6.125	1.350	5000	6.608	3.400	5000
6.175	1.500	5000	6.664	3.800	5000
6.195	1.550	5000	6.740	4.400	5000
6.245	1.700	5000	6.800	4.900	5000
6.260	1.750	5000	6.880	5.700	5000
6.285	1.850	5000	6.950	6.550	5000
6.315	1.950	5000	7.030	7.550	5000
6.341	2.050	5000	7.150	5.000	1000
6.354	2.100	5000	7.280	5.000	1000
6.390	2.250	5000	7.373	5.000	1000
6.423	2.400	5000	7.500	2.100	1000
6.445	2.500	5000	7.596	5.000	1000
6.460	2.550	5000	7.825	5.000	1000
6.488	2.700	5000	8.000	25.000	1000
6.515	2.850	5000	8.200	6.700	1000
6.550	3.050	5000	8.400	9.400	1000

TABLE VII. $32^3 \times 8$ gauge configurations used for the gradient flow analysis.

β	$t_{\max}$	# TU	β	$t_{\max}$	# TU
6.664	3.800	3230	7.200	10.350	3600
6.700	4.100	5000	7.280	11.950	1000
6.740	4.400	5000	7.373	14.150	5000
6.770	4.650	5000	7.500	2.050	1000
6.800	4.900	5000	7.596	2.400	5000
6.840	5.300	5000	7.650	2.650	1000
6.860	5.500	5000	7.825	5.000	1000
6.880	5.700	5000	8.000	5.000	1000
6.910	6.050	4120	8.200	7.000	1000
6.950	6.500	5000	8.400	10.000	1000
6.990	7.050	5000	8.570	12.500	1000
7.030	7.550	5000	8.710	15.800	1000
7.150	9.450	1000	8.850	19.950	1000

TABLE IX. $48^3 \times 12$ gauge configurations used for the gradient flow analysis.

[15] A. Mykkanen, M. Panero, and K. Rummukainen, JHEP **05**, 069 (2012), 1202.2762.

Scheme	β	n_k, sm	$\frac{\chi^2}{\mathrm{d}f}$	n_p	$\frac{\chi^2}{\mathrm{d}f}$
$Q\bar{Q}$ procedure					
0th iteration	[5.900,7.825]	5, 0.18	0.30		
Direct renormalization					
1st iteration	[5.900,8.850]	5, 0.04	0.83		
2nd iteration	[5.900,9.670]	6, 0.03	0.28	5	0.17

TABLE X. Spline and polynomial interpolations of c_Q.

[16] Y. Burnier, M. Laine, and M. Vepsalainen, JHEP **01**, 054 (2010), [Erratum: JHEP 01, 180 (2013)], 0911.3480.
[17] M. Berwein, N. Brambilla, P. Petreczky, and A. Vairo (2015), 1512.08443.
[18] P. Petreczky and K. Petrov, Phys. Rev. **D70**, 054503 (2004), hep-lat/0405009.
[19] O. Kaczmarek and F. Zantow, Phys. Rev. **D71**, 114510 (2005), hep-lat/0503017.
[20] M. Cheng *et al.*, Phys. Rev. **D77**, 014511 (2008), 0710.0354.
[21] A. Bazavov *et al.*, Phys. Rev. **D80**, 014504 (2009), 0903.4379.
[22] M. Cheng *et al.*, Phys. Rev. **D81**, 054504 (2010), 0911.2215.

N_τ	T [MeV]	β	n_k, sm	$\frac{\chi^2}{\mathrm{d}f}$	n_p	$\frac{\chi^2}{\mathrm{d}f}$
4	[201,5814]	[5.900,9.670]	18, 0.0	0.93	9	0.71
6	[234,237]	[5.900,6.488]	7, 0.05	0.90	9	0.79
6	[181,3876]	[6.215,9.670]	19, 0.0	1.03	9	1.06
8	[116,227]	[6.050,6.740]	6, 0.0	1.01	7	0.73
8	[201,2907]	[6.515,9.670]	15, 0.0	0.87	9	1.07
10	[116,239]	[6.285,7.030]	6, 0.0	0.86	6	0.83
10	[181,924]	[6.740,8.570]	8, 0.0	1.06	7	1.01
12	[122,233]	[6.515,7.200]	5, 0.05	0.88	4	0.85
12	[185,974]	[6.950,8.850]	8, 0.0	0.96	7	1.00

TABLE XI. Primary spline and polynomial interpolations of f_Q^{bare}.

$\{n_0, n_2, n_4\}$	$N_\tau^{\min}$	T [MeV]	$\frac{\chi^2}{\mathrm{d}f}$	$R[12]$	$R[10]$	$R[8]$	$R[6]$
$\{6,5,0\}$	8	[115,215]	0.26	0.30	0.26	0.22	–
$\{6,5,4\}$	6	[115,225]	0.24	0.21	0.30	0.34	0.10
$\{5,3,0\}$	8	[173,410]	0.21	0.36	0.25	0.04	–
$\{5,3,0\}$	6	[173,410]	0.28	0.62	0.17	0.27	0.10

TABLE XII. Global continuum extrapolations using $Q\bar{Q}$ procedure. The last four columns denote $R[N_\tau] = \frac{\chi^2(N_\tau)}{n_{\mathrm{pt}}(N_\tau)}$, the ratio of residues and number of points for each N_τ.

T [MeV]	F_Q [MeV]	S_Q	T [MeV]	F_Q [MeV]	S_Q
125	481(7)	1.99(56)	280	144(5)	1.21(07)
130	470(6)	2.00(49)	290	132(5)	1.14(06)
135	459(5)	2.29(40)	300	121(6)	1.07(06)
140	446(4)	2.78(34)	310	113(5)	0.99(06)
145	431(4)	3.26(29)	320	103(6)	0.94(06)
150	413(4)	3.60(24)	330	94(6)	0.90(06)
155	395(4)	3.67(20)	340	85(6)	0.87(05)
160	377(4)	3.47(20)	350	76(6)	0.85(05)
165	360(4)	3.19(18)	360	68(7)	0.82(05)
170	345(4)	2.94(15)	370	59(7)	0.80(05)
175	330(4)	2.83(15)	380	50(6)	0.80(05)
180	317(4)	2.75(15)	390	42(6)	0.77(05)
185	303(4)	2.56(15)	400	34(6)	0.75(05)
190	291(4)	2.45(13)	410	27(6)	0.74(05)
200	268(4)	2.15(13)	420	19(6)	0.72(05)
210	248(4)	1.89(11)	430	12(7)	0.71(05)
220	231(4)	1.72(12)	440	6(7)	0.69(05)
230	214(5)	1.67(10)	450	-1(7)	0.68(05)
240	198(5)	1.60(10)	460	-8(7)	0.66(05)
250	182(5)	1.52(10)	470	-14(7)	0.64(05)
260	170(4)	1.38(08)	480	-20(8)	0.63(05)
270	157(5)	1.30(08)	490	-26(8)	0.61(05)

T [MeV]	F_Q [MeV]	S_Q	T [MeV]	F_Q [MeV]	S_Q
500	-32(8)	0.60(06)	940	-202(20)	0.33(04)
520	-44(8)	0.57(06)	960	-209(20)	0.32(04)
540	-55(8)	0.55(06)	980	-215(21)	0.32(04)
560	-66(9)	0.53(06)	1000	-221(21)	0.31(04)
580	-76(9)	0.51(06)	1100	-251(24)	0.28(03)
600	-86(9)	0.49(07)	1200	-277(25)	0.24(04)
620	-96(9)	0.47(07)	1300	-301(25)	0.23(04)
640	-105(9)	0.45(06)	1400	-323(25)	0.21(04)
660	-114(10)	0.43(06)	1500	-343(27)	0.19(04)
680	-122(11)	0.41(06)	1600	-362(28)	0.18(05)
700	-130(12)	0.41(04)	1700	-390(30)	0.17(06)
720	-138(12)	0.40(05)	1800	-397(31)	0.16(06)
740	-145(13)	0.40(05)	1900	-413(32)	0.16(06)
760	-152(13)	0.39(05)	2000	-430(32)	0.16(06)
780	-159(14)	0.38(05)	2400	-501(34)	0.17(03)
800	-165(14)	0.38(05)	2800	-584(47)	0.15(02)
820	-171(14)	0.37(05)	3200	-664(45)	0.14(03)
840	-177(15)	0.36(05)	3600	-717(47)	0.13(04)
860	-182(15)	0.36(05)	4000	-768(49)	0.12(03)
880	-187(15)	0.35(05)	4400	-817(52)	0.12(03)
900	-192(15)	0.34(05)	4800	-867(51)	0.13(03)
920	-196(16)	0.33(05)	5200	-929(54)	0.15(06)

TABLE XIII. Continuum limit of the free energy F_Q and entropy S_Q for high temperatures. F_Q is a shifted finite N_τ result above $T > 920$ MeV. For $T \leq 2800$ MeV, $N_\tau = 8$ is used and for $T > 2800$ MeV $N_\tau = 4$ is used. The cutoff effects at $T = 920$ MeV are used as shift and added to the errors linearly. S_Q is a finite N_τ result above $T > 680$ MeV. For $T \leq 2000$ MeV, $N_\tau = 8$ is used and for $T > 2000$ MeV $N_\tau = 4$ is used. Errors of S_Q for the finite N_τ result are increased by 0.01.

[23] S. Borsanyi, Z. Fodor, C. Hoelbling, S. D. Katz, S. Krieg, C. Ratti, and K. K. Szabo (Wuppertal-Budapest), JHEP **09**, 073 (2010), 1005.3508.

[24] A. Bazavov *et al.*, Phys. Rev. **D85**, 054503 (2012), 1111.1710.

[25] A. Bazavov and P. Petreczky, Phys.Rev. **D87**, 094505 (2013), 1301.3943.

[26] Borsanyi, Szabolcs and Fodor, Zoltan and Katz, Sándor D. and Pásztor, Attila and Szabó, Kálmán K. and Török, Csaba, JHEP **04**, 138 (2015), 1501.02173.

[27] S. Borsanyi, S. Durr, Z. Fodor, C. Holbling, S. Katz, S. Krieg, D. Nogradi, K. Szabo, B. Toth, and N. Trombitas, Phys. Rev. **D92**, 014505 (2015), 1504.03676.

[28] S. Borsanyi, Z. F. S. D. K. S. Krieg, T. Lippert, D. Nogradi, F. Pittler, K. K. Szabo, and B. C. Toth (2015), 1510.03376.

[29] F. Karsch, E. Laermann, and A. Peikert, Nucl. Phys. **B605**, 579 (2001), hep-lat/0012023.

[30] Y. Aoki, Z. Fodor, S. D. Katz, and K. K. Szabo, Phys. Lett. **B643**, 46 (2006), hep-lat/0609068.

[31] Y. Aoki, S. Borsanyi, S. Durr, Z. Fodor, S. D. Katz, S. Krieg, and K. K. Szabo, JHEP **06**, 088 (2009), 0903.4155.

[32] P. M. Lo, B. Friman, O. Kaczmarek, K. Redlich, and C. Sasaki, Phys. Rev. **D88**, 074502 (2013), 1307.5958.

[33] E. Follana, Q. Mason, C. Davies, K. Hornbostel, G. P. Lepage, J. Shigemitsu, H. Trottier, and K. Wong (HPQCD, UKQCD), Phys. Rev. **D75**, 054502 (2007), hep-lat/0610092.

[34] A. Bazavov *et al.* (HotQCD), Phys. Rev. **D90**, 094503 (2014), 1407.6387.

[35] H. T. Ding, S. Mukherjee, H. Ohno, P. Petreczky, and H. P. Schadler, Phys. Rev. **D92**, 074043 (2015), 1507.06637.

[36] A. Bazavov, H. T. Ding, P. Hegde, F. Karsch, C. Miao, S. Mukherjee, P. Petreczky, C. Schmidt, and A. Velytsky, Phys. Rev. **D88**, 094021 (2013), 1309.2317.

[37] A. Bazavov *et al.* (MILC), Phys. Rev. **D82**, 074501 (2010), 1004.0342.

[38] A. M. Polyakov, Nucl. Phys. **B164**, 171 (1980).

[39] E. Megias, E. Ruiz Arriola, and L. L. Salcedo, Phys. Rev. Lett. **109**, 151601 (2012), 1204.2424.

[40] O. Kaczmarek and F. Zantow (2005), hep-lat/0506019.

[41] D. E. Kharzeev, Phys. Rev. **D90**, 074007 (2014), 1409.2496.

[42] K. Hashimoto and D. E. Kharzeev, Phys. Rev. **D90**, 125012 (2014), 1411.0618.

[43] P. Petreczky, *Proceedings, 1st International Conference on Hard and Electromagnetic Probes of High-Energy Nuclear Collisions (Hard Probes 2004)*, Eur. Phys. J. **C43**, 51 (2005), hep-lat/0502008.

[44] M. Luscher, JHEP **08**, 071 (2010), [Erratum: JHEP03,092(2014)], 1006.4518.

[45] M. Luscher and P. Weisz, JHEP **02**, 051 (2011), 1101.0963.

[46] S. Borsanyi *et al.*, JHEP **09**, 010 (2012), 1203.4469.

[47] A. Bazavov *et al.* (MILC) (2015), 1503.02769.

[48] M. Asakawa, T. Hatsuda, E. Itou, M. Kitazawa, and H. Suzuki (FlowQCD), Phys. Rev. **D90**, 011501 (2014), [Erratum: Phys. Rev.D92,no.5,059902(2015)], 1312.7492.

[49] P. Petreczky and H. P. Schadler, Phys. Rev. **D92**, 094517 (2015), 1509.07874.

[50] S. Datta, S. Gupta, and A. Lytle (2015), 1512.04892.

[51] P. M. Lo, B. Friman, O. Kaczmarek, K. Redlich, and C. Sasaki, Phys. Rev. **D88**, 014506 (2013), 1306.5094.

[52] A. Bazavov, N. Brambilla, X. Garcia i Tormo, P. Petreczky, J. Soto, and A. Vairo, Phys. Rev. **D90**, 074038 (2014).

[53] A. Bazavov, N. Brambilla, X. Garcia i Tormo, P. Petreczky, J. Soto, and A. Vairo, Phys. Rev. **D86**, 114031 (2012), 1205.6155.

[54] R statistical package, `http://www.r-project.org/`.